



HAL
open science

Type VI secretion TssK baseplate protein exhibits structural similarity with phage receptor-binding proteins and evolved to bind the membrane complex

van Son Nguyen, Laureen Logger, Silvia Spinelli, Pierre Legrand, Thi Thanh Huyen Pham, Thi Trang Nhung Trinh, Yassine Cherrak, Abdelrahim Zoued, Aline Desmyter, Eric Durand, et al.

► To cite this version:

van Son Nguyen, Laureen Logger, Silvia Spinelli, Pierre Legrand, Thi Thanh Huyen Pham, et al.. Type VI secretion TssK baseplate protein exhibits structural similarity with phage receptor-binding proteins and evolved to bind the membrane complex. *Nature Microbiology*, 2017, 2, pp.17103. 10.1038/nmicrobiol.2017.103 . hal-01780712

HAL Id: hal-01780712

<https://amu.hal.science/hal-01780712>

Submitted on 27 Apr 2018

HAL is a multi-disciplinary open access archive for the deposit and dissemination of scientific research documents, whether they are published or not. The documents may come from teaching and research institutions in France or abroad, or from public or private research centers.

L'archive ouverte pluridisciplinaire **HAL**, est destinée au dépôt et à la diffusion de documents scientifiques de niveau recherche, publiés ou non, émanant des établissements d'enseignement et de recherche français ou étrangers, des laboratoires publics ou privés.

1 **Type VI secretion TssK baseplate protein exhibits structural similarities with phage**
2 **receptor binding protein and evolved to bind the membrane complex**

3

4 Van Son Nguyen^{1,2}, Laureen Logger³, Silvia Spinelli^{1,2}, Pierre Legrand⁴, Thi Thanh Huyen
5 Pham^{1,2,5}, Thi Trang Nhung Trinh^{1,2,5}, Yassine Cherrak³, Abdelrahim Zoued³, Aline
6 Desmyter^{1,2}, Eric Durand³, Alain Roussel^{1,2}, Christine Kellenberger^{1,2}, Eric Cascales^{3*} and
7 Christian Cambillau^{1,2*}

8

9 ¹ Architecture et Fonction des Macromolécules Biologiques, Aix-Marseille Université,
10 Campus de Luminy, Case 932, 13288 Marseille Cedex 09, France.

11 ² Architecture et Fonction des Macromolécules Biologiques, Centre National de la Recherche
12 Scientifique (CNRS), Campus de Luminy, Case 932, 13288 Marseille Cedex 09, France.

13 ³ Laboratoire d'Ingénierie des Systèmes Macromoléculaires, Institut de Microbiologie de la
14 Méditerranée, Aix-Marseille Univ. - Centre National de la Recherche Scientifique
15 (UMR7255), 31 Chemin Joseph Aiguier, 13402 Marseille Cedex 20, France.

16 ⁴ Synchrotron Soleil, L'Orme des Merisiers, Saint-Aubin - BP 48, 91192 Gif-sur-Yvette
17 Cedex, France.

18 ⁵ University of Science and Technology of Hanoi, Training and Services Building, Vietnam
19 Academy of Science and Technology, 18 Hoang Quoc Viet, Cau Giay District, Hanoi,
20 VietNam

21

22 * corresponding authors: Eric Cascales (cascales@imm.cnrs.fr) and Christian Cambillau
23 (cambillau@afmb.univ-mrs.fr).

24 *Running title:* T6SS-bacteriophage baseplate homology

25 *Keywords:* Type VI secretion, nanobody, protein secretion, protein transport, baseplate,

26 structure-function analysis, contractile tail, receptor binding protein, shoulder, tail assembly

27

28 **ABSTRACT**

29

30 **The Type VI secretion system (T6SS) is a multiprotein machine widespread in**
31 **Gram-negative bacteria that delivers toxins into both eukaryotic and prokaryotic cells.**
32 **The mechanism of action of the T6SS is comparable to that of contractile myophages.**
33 **The T6SS builds a tail-like structure made of an inner tube wrapped by a sheath**
34 **assembled under an extended conformation. Contraction of the sheath propels the inner**
35 **tube toward the target cell. The T6SS tail is assembled on a platform – the baseplate –**
36 **functionally similar to bacteriophage baseplates. In addition, the baseplate docks the tail**
37 **to a trans-envelope membrane complex that orients the tail toward the target. Here, we**
38 **report the crystal structure of TssK, a central component of the T6SS baseplate. We**
39 **show that TssK is constituted of three domains and establish the contribution of each**
40 **domain to the interaction with TssK partners. Importantly, this study reveals that the**
41 **N-terminal domain of TssK is structurally homologous to the shoulder domain of phage**
42 **receptor binding proteins while the C-terminal domain binds the membrane complex.**
43 **We propose that TssK has conserved the domain of attachment to the virion particle but**
44 **has evolved the reception domain to use the T6SS membrane complex as receptor.**

45 **Introduction**

46 Delivery of bacterial effector proteins and toxins into target cells relies on trans-
47 envelope nanomachines called secretion systems. These machines select and transport
48 effectors in the milieu or directly into the target cell¹. Most of these secretion systems evolved
49 from efflux pumps or from machineries involved in conjugation or flagellar, twitching or
50 gliding motility¹. The Type VI secretion system (T6SS) is a fascinating machine that uses a
51 contractile mechanism similar to that of contractile tail structures such as bacteriophages or
52 R-pyocins²⁻⁷. The T6SS delivers toxins and effectors in both eukaryotic and procaryotic cells
53 and participates to bacterial pathogenesis and inter-bacterial competition^{8,9}. By eliminating
54 competing bacteria, the T6SS confers an increased ability to colonize the niche¹⁰⁻¹⁶
55 Basically, the T6SS can be viewed as a contractile tail oriented towards the target cell and
56 anchored to the cell envelope by a membrane complex (MC)^{3,17}. The MC is evolutionarily
57 related to a sub-complex associated with Type IVb secretion system^{18,19}. The MC is a 1.7-
58 MDa trans-envelope structure constituted of three conserved subunits: the TssJ outer
59 membrane lipoprotein and the TssL and TssM inner membrane proteins²⁰⁻²⁶. In several cases,
60 the MC is properly inserted and anchored to the cell wall by additional proteins with
61 peptidoglycan hydrolysis and peptidoglycan binding properties^{21,27-29}. The contractile tail is
62 composed of the inner tube made of hexamers of the Hcp protein, stack on each other^{30,31},
63 tipped by VgrG and surrounded by the contractile sheath made of the TssBC proteins³⁰⁻³². The
64 polymerization of the tail tube/sheath tubular structure is initiated on an assembly platform,
65 the baseplate (BP), the less characterized T6SS sub-complex, and is coordinated by the TssA
66 protein³³⁻³⁵. The T6SS contractile tail shares functional and structural homologies with the tail
67 of several bacteriophages^{5,6,30,36,37}. Once the T6SS tail is assembled, the sheath contracts and
68 propels the inner tube/spike needle complex towards the target cell³⁹⁻⁴², and it has been
69 proposed that this needle complex traverses the cell envelope through the MC²⁶. A recent *in*

70 *in vivo* study identified five components of the BP: TssE, –F, –G, –K and VgrG³⁴. While TssA
71 was also identified in this screen, later observations have demonstrated that TssA is not a
72 structural component of the baseplate *per se*³⁴. TssE is a homologue of gp25, a bacteriophage
73 T4 baseplate wedge protein^{18,19,43}. By contrast, no tri-dimensional structure is available for
74 TssF, –G or –K. *In silico* analyses recently predicted that TssF and TssG share limited
75 homologies with gp6 and gp7 respectively³⁴ whereas controversies exist regarding TssK^{44,45}.
76 Interestingly, T6SS BP sub-complexes could be isolated in *Serratia marcescens* and
77 uropathogenic *Escherichia coli* (UPEC) such as the TssKFG or TssKFGE complexes^{33,45}.
78 These complexes likely represent the equivalent of wedge complexes of phage baseplates,
79 which assemble around the central gp27-gp5 hub/spike^{46,47}. In addition to appear central for
80 the assembly of the T6SS wedges, TssK is a key BP subunit mediating contacts with the
81 cytoplasmic domains of MC components^{35,48,49}. Hence, TssK is an essential BP component
82 connecting MC, BP and tail components. However, we still lack structural information on
83 TssK. While we showed that TssK assembles trimeric complexes in enteroaggregative *E. coli*
84 (EAEC)⁴⁸, a study reported that it assembles trimers and hexamers in *S. marcescens*³³. The
85 available structural information on the EAEC TssK protein (accession number: EC042_4526)
86 consists to the low-resolution (~ 26 Å) negative stained electron microscopy structure of the
87 TssK trimer, as well as its SAXS envelope⁴⁸. Despite intensive efforts, neither full-length of
88 cleaved forms of TssK could be crystallized. Here, we report the crystal structure of the full-
89 length EAEC TssK protein, obtained as a complex with a camelid nanobody that facilitated
90 the crystallisation process. The structure of trimeric TssK reveals an unexpected homology of
91 its N-terminal domain with siphophages RBP shoulders, hence expanding the number of
92 homologous proteins between T6SS and bacteriophages. While TssK N-terminal domain
93 attaches to the rest of T6SS baseplate, the C-terminal domain binds the membrane complex
94 and has evolved to use the T6SS membrane complex as receptor for docking the baseplate. In

95 addition, the flexibility of the TssK C-terminal domain suggests that TssK may establish a
96 flexible link to maintain the anchorage of the baseplate to the T6SS membrane complex
97 before and after tail contraction.

98

99 **Results**

100

101 *TssK crystallization is facilitated when complexed to the TssK-specific nb18 nanobody.*

102 Despite extensive efforts, previous attempts to crystallize TssK were unsuccessful.
103 Crystallization of proteins has been previously shown to be facilitated once the protein of
104 interest is complexed to camelid single-chain antibodies, called nanobodies⁵⁰. We used this
105 approach for the crystallization of the periplasmic domain of the T6SS TssM subunit^{26,51,52}.
106 We therefore immunized a llama with purified TssK, and isolated nanobodies that bind TssK:
107 nbK18, nbK25 and nbK27. The crystal structure of nbK18 was determined (Supplementary
108 Figure 1a) and its complexation with TssK was then monitored by Biolayer interferometry
109 (BLI). Kinetic and steady-state analyses defined K_D of 2.4 nM and 3.1 nM respectively.

110

111 *The TssK structure reveals a three-domain protein organized as a tightly packed trimer.*

112 The structure of the nbK18-TssK co-crystallized complex was determined at 2.6 Å
113 resolution. The complex contains three TssK molecules to which three nbK18 units are bound
114 (Supplementary Figure 1b). TssK trimerization is in agreement with previous gel filtration
115 data suggesting that TssK forms trimer⁴⁸. Each nanobody interacts with two monomers of
116 TssK and covers $\sim 700 \text{ \AA}^2$ of the accessible surface area of a TssK monomer and 80 \AA^2 of a
117 second monomer. Interaction of nbK18 with TssK is mainly mediated by nbK18 CDR3 but
118 also by the two other CDRs and the conserved skeleton (Supplementary Figure 1b,

119 Supplementary Table 2), a feature already observed in other cases^{53,54}. NbK18 binds the TssK
120 N-terminal β -sandwich and more specifically the L4-5 and L6-7 loops (Supplementary
121 Figure 1b inset; Supplementary Table 2).

122 The TssK trimer has the overall structure of an apple core or an hourglass, with two globular
123 domains – the N-terminal shoulder (hereafter named TssK_S) and C-terminal head (TssK_H)
124 domains – separated by a helical stalk, the neck (TssK_N). The TssK trimer is tightly packed,
125 as 1400-1570 Å² of the accessible surface area of each monomer is covered by the two other
126 monomers (Fig. 1a). The structure exhibits high B-factors (~ 100 Å²) and consequently the
127 side-chains of solvent exposed residues are often disordered when not involved in crystal
128 packing contacts. A large segment is missing at the bottom of the shoulder domain, between
129 residues 130 and 144, and a short loop is incomplete at the top of the neck domain, between
130 residues 221 and 224. These segments have not been incorporated into the model (Fig.
131 1a). Two of the three monomers are not complete: their amino acid chains start at residue 19
132 and end at residues 320 and 315 for monomers A and C, respectively, suggesting that their C-
133 terminal domain might be totally disordered. In contrast, the main-chain of monomer B could
134 be traced up to residue 334, and the side-chain identity can be assigned (Fig. 1a). However,
135 despite its stabilization by crystal contacts, the C-terminal domain of chain B exhibits an
136 average B-factor double compared to the rest of the structure, impeding its complete
137 assignment (Fig. 1a).

138 The TssK monomer structure comprises three domains: a N-terminal β -sandwich domain
139 (shoulder, TssK_S, residues 19-174), a linker (residues 175-193) and a four-helix bundle
140 middle domain (neck, TssK_N, residues 194-313), and, in chain B only, a partially traced C-
141 terminal domain (head, TssK_H, residues 315-447) (Fig. 1b). The N-terminal domain starts
142 with a long α -helix followed by three anti-parallel β -strands forming a β -sheet (β 1- β 3). After
143 β -strand 4, a short β -hairpin (β 4, β 5) is followed by β -strands 6 and 7. Together, β -strands 4, 6

144 and 7 form the second β -sheet of the β -sandwich. After a long linker, α -helices 2, 3 and 4
145 form an antiparallel bundle. Helix 4 is then followed by a long unstructured stretch of
146 residues returning in the direction of the N-terminus and positioning α -helix 5 parallel to α -
147 helix 3, allowing the chain to continue in a direction opposite to the N-terminus. The C-
148 terminal domain, starting at residue 317, is predicted by JPRED⁵⁵ as assembling three α -
149 helices and seven β -strands. We assigned 106 amino acids for a total of 125 for the complete
150 C-terminal domain. At this stage it comprised two complete α -helices and an incomplete one,
151 as well as two β -sheets forming a β -sandwich of putatively 7 β -strands, but most connections
152 were not visible in the electron density map.

153 To obtain a better model of TssK, the C-terminal domain (amino-acids 316-445) was
154 produced, crystallized and its structure solved at 1.6 Å resolution. This domain is very
155 compact and comprises three α -helices (α 6-8) and 7 β -strands (β 10-16) (Fig. 1b). The
156 structure of the isolated C-terminal domain was reintroduced in the structure of full-length
157 TssK, and refinement was performed. Apart from loop 372-382, which has a different
158 conformation, the domain conformations are very close in the isolated and full-length
159 structures (r.m.s.d = 1.2 Å on 115 residues) (Supplementary Figure 2). Notably, the C-
160 terminal domain of chain B establishes stabilizing packing contacts, involving mainly loop
161 372-382. As such, the complete TssK trimer is ~110 Å long and ~85 Å wide at the level of
162 the shoulder domains, and ~40 Å wide at the level of the central domain (Fig. 1a).

163 We previously reported the negative stain electron microscopy (EM) structure of TssK⁴⁸. The
164 crystal structure of TssK was fitted into the EM map using Chimera⁵⁶ (Fig. 1c,d). With the
165 exception of the C-terminal domain of monomer B, TssK fits exquisitely well into the EM
166 structure with a correlation of 0.89 and 93 % of atoms included in the map.

167 Nanobody epitope analysis performed by BLI revealed that nbK27 and nbK25 bind
168 TssK using another epitope compared to nbK18. We therefore co-crystallized the cloned

169 TssK_{SN} domain (shoulders and neck domain, residues 1-315) with nbK18 and nbK27. Crystals
170 of the TssK_{SN}-nbK18–nbK27 were obtained and the structure was solved (Supplementary
171 Table 1). The structure of the TssK_{SN}-nbK18–nbK27 superimposes well with that of the
172 TssK-nbK18 complex, with a small rotation of the three nbK18. By contrasts to nbK18, that
173 binds each TssK monomer, a unique nbK27 binds the trimeric assembly along the 3-fold axis
174 at the bottom of the shoulder domains (Fig. 2a,b), resulting in a TssK₃/nbK18₃/nbK27₁
175 stoichiometry. The most striking result of nbK27 binding to TssK is the ordering of the
176 bottom of the shoulder domains segments that were disordered in the TssK-nbK18 complex:
177 the N-terminal segment 1-19 and the β-hairpin 130-144 (Fig. 2c,d). This ordering results in
178 strong domain-swapped like interactions of the 1-19 segment with the i-1 monomer, and of
179 the 130-144 β-hairpin with the i+1 monomer (Fig. 2c). Notably, the stabilized structures
180 comprise all the bottom part of TssK, a surface with a diameter of ~50 Å (Fig. 2d). Finally,
181 the list of domains or segments present in the different crystal structures is summarized as a
182 linear sequence representation with secondary structures (Supplementary Figure 3).

183

184 *The TssK N-terminal domain shares structure similarities with phage Receptor Binding*
185 *Protein shoulder domains.*

186 The three domains of TssK were subjected to DALI analyses to detect structural
187 similarities. Interestingly, DALI retrieved strong similarities between the TssK N-terminal β-
188 sandwich domain and the shoulder domains from lactococcal siphophages receptor binding
189 proteins (RBP) (Fig. 3), including phages 1358 (PDB: 4L9B, Z=9.0, r.m.s.d. = 3.0 Å;⁵⁷) and
190 p2 (PDB: 1ZRU, Z=6.0 r.m.s.d.= 3.0 Å;⁵⁸). In addition, although helix bundles represent a
191 common structural fold, DALI analyses detected similarities between the TssK neck domain
192 and a domain of the human adenylosuccinate lyase (PDB: 4FFX, Z=9.4, r.m.s.d.=3.1 Å;⁵⁹)
193 (Supplementary Figure 4).

194

195 *Interaction analyses of TssK domains*

196 Previous studies have shown that TssK is a central subunit of the T6SS, as it interacts
197 with components of the MC (the cytoplasmic domains of TssL (TssL_C) and TssM (TssM_C)),
198 of the baseplate (the TssFG complex) and of the tail (TssA, TssC and Hcp)^{33,34,39,48,60}. We
199 therefore sought to define the domains mediating TssK interactions with MC and BP. First,
200 the N-terminal shoulder and neck (TssK_{SN}), shoulder (TssK_S), neck (TssK_N) and C-terminal
201 head (TssK_H) domains of TssK were cloned in two-hybrid vectors and tested for their ability
202 to promote oligomerization and to interact with TssFG, TssL_C and TssM_C (Fig. 4a). In
203 agreement with the crystal structure of the TssK trimer (Fig. 1a), both shoulder and neck
204 domains oligomerize whereas the TssK head domain does not interact with TssK (Fig. 4a,
205 first column). More interestingly, the two-hybrid analyses revealed that the N-terminal
206 shoulder domain mediates contacts with the TssFG complex whereas the C-terminal head
207 domain interacts with TssL_C, TssM_C and to a lesser extent to TssFG. We then monitored co-
208 immunoprecipitation experiments. Soluble lysates of cells producing the VSV-G-tagged TssK
209 domains were combined with lysates containing FLAG-tagged TssF and TssG, or the
210 cytoplasmic domains of TssL (TssL_C) or TssM (TssM_C). FLAG-tagged proteins were
211 immobilized on agarose beads coupled to the monoclonal anti-FLAG antibody and the eluted
212 material was analysed by SDS-PAGE and immuno-staining. Figure 4b shows that the TssK_S
213 domain is co-precipitated with the TssFG complex, whereas the the TssK_H domain co-
214 precipitates with TssL_C and TssM_C - and to a lower extent - with TssFG. The results of
215 BACTH and co-immunoprecipitation analyses are summarized in Supplementary Figure 5.

216 To confirm these results, we engineered vectors producing TssFG as well as either
217 6×His-tagged TssK_{SN} or TssK_H. HPLC chromatography indicated that TssKFG and
218 TssK_{SN}FG complexes form (Supplementary Figure 6a). However, while we succeeded to

219 purify the TssK_{SN}FG complex (Fig. 4c, Supplementary Figure 6a), TssK_H was purified alone
220 and did not co-purify with TssFG; isolated TssFG is not observed on the chromatogram as it
221 is insoluble (Supplementary Figure 7a). These results confirm the TssK_{SN}/TssFG complex
222 interaction and indicate that the low TssK_H/TssFG interaction, observed by BACTH and co-
223 immuno-precipitation, should be weaker and in fast exchange. To gain further insights on the
224 contribution of the TssK_{SN} domain for binding to the TssFG complex, we then tested binding
225 of the TssK-specific nbK18 and nbK27 nanobodies to the TssK_{SN}FG complex. The purified
226 TssK_{SN}FG complex was mixed with an excess of nanobody and analysed by gel filtration and
227 HPLC. First, we confirmed that nbK18 and nbK27 bind alone and simultaneously to TssK_{SN}.
228 We performed then the analysis of TssK_{SN}FG in the presence of nbK18, nbK27 and nbK18 +
229 nbK27 (Supplementary Figure 6b). We found that nbK18 binds to the TssK_{SN}FG complex
230 (Fig. 4c,d and Supplementary Figure 6c) whereas nbK27 does not (Fig. 4c,e). From these
231 results, we concluded that nbK27 and TssFG share the same binding site to TssK, and hence,
232 that TssFG should bind to the bottom of the TssK_S domain comprising the residues 1-19
233 segment and the 130-144 β -hairpin. Taken together, the results of the co-purification and the
234 nanobody binding experiments confirmed the interaction of TssK_S with the TssFG complex
235 and suggested that TssFG binds the bottom of TssK_S.
236 We could not assay the TssK_H interaction with the TssMc domain, as it is insoluble. In
237 contrast we performed a gel filtration of a mixture of TssLc and TssK_H, and found that they
238 do not co-purify. As an interaction is observed by double-hybrid and co-immunoprecipitation
239 this latter result suggests that this interaction is rather weak (around 1-10microM) and in fast
240 exchange. Indeed, this does not reflect the biological situation in which the interaction of
241 several TssK trimers and several Lc dimers occurs, leading certainly to a tremendous avidity
242 increase.
243

244 **Discussion**

245 In this work, we present the crystal structure and a domain analyses of a T6SS core
246 component, TssK. Previous studies have demonstrated that TssK is a trimer and is an
247 essential subunit of the Type VI secretion apparatus by connecting the trans-envelope
248 membrane complex to the phage-like contractile tail⁴⁸. In addition, TssK has been shown to
249 be part of the T6SS assembly platform or baseplate^{33,34,39,45,48}. It has been recently reported
250 that phage T4 is a very complex phage, and that phage Mu is a simpler, widespread, and a
251 better paradigm of phages with contractile tails⁶¹. Notably, TssK has no counterpart in phage
252 Mu whereas other T6SS baseplate components have counterparts in both phages T4⁴⁵ and
253 Mu⁶¹: TssE corresponds to gp25 (T4) and Mup46 (Mu), TssF to gp6 and Mup47 and TssG to
254 Mup48 (no homologue in T4).

255 The X-ray structure of TssK confirms that TssK exists as a trimer. The TssK trimer
256 has an overall architecture resembling that of an apple core: a shoulder base and a distal head
257 separated by the central neck. The structure of TssK is modular. It comprises three domains: a
258 N-terminal domain, essentially β -stranded, comparable to the N-terminal shoulder domains of
259 phages p2 and 1358 RBPs, followed by a α -helical central domain and a mixed $\alpha\beta$ C-
260 terminal globular domain. *In vivo* interactions studies with known partners of TssK support
261 the idea that TssK acts as a connector between two T6SS complexes that are evolutionarily
262 unrelated: the phage-like baseplate/tail and the T4bSS IcmF/DotU-like membrane complex
263 (Fig. 5). From the protein-protein interaction assays we concluded that the TssK N-terminal
264 shoulder domain binds to TssFG and that the C-terminal head domain mediates interactions
265 with the TssL and TssM inner membrane proteins..

266 The fascinating observation of this study is that TssK shares a similar overall
267 architecture with lactococcal siphophage receptor-binding proteins. These RBPs are trimers
268 and comprise shoulder and head domains separated by the neck^{57,58,62}. They recognize the

269 host cell surface and are responsible for properly orienting the phage onto the host cell^{63,64}.
270 RBPs are anchored to the virion and bind to receptors at the cell surface of the target cell.
271 Anchorage to the virion particle is mediated by the shoulder domain whereas the ability to
272 recognize the cell envelope receptor is conferred by the head domain. It has been reported that
273 in each lactococcal phage family, the shoulder domain structure is strictly conserved whereas
274 the head domain is relatively diverse and confers specificity for binding to the proper target
275 cell^{57,58,62,63,65}. Another striking similarity between the TssK and RBP shoulder domains is the
276 ordering of their bottom segments upon binding to partners. When the phage p2 RBP is
277 expressed alone, the 20 N-terminal residues are disordered and not visible in the electron map
278 density. In contrast, they are ordered when the RBP is complexed with the other baseplate
279 components and constitutes the main contributors to the interaction. Worth noticing, the “arm
280 and hand” domain of the Dit protein inserts between the three N-termini, holding thus the
281 RBP trimer^{58,62,65}. A similar situation may exist with TssK. Although we do not have the
282 structure of TssK within the TssKFG complex, nanobody binding experiments on the
283 TssKFG complex have shown that the TssFG binding site on TssK involves the bottom of the
284 trimer, including the N-termini (Supplementary Figure 8). The ordering of this site upon
285 nbK27 binding suggests that this nanobody acts as a surrogate of the TssFG complex.
286 In myophages, such as phages T4 or Mu, both the baseplate and the tail sheath change
287 conformation upon contraction^{45,61}. The tail sheath conformational change is also
288 documented for the T6SS³². It is therefore expected that a conformational reorganization also
289 occurs for the T6SS baseplate^{35,38}. The flexibility of TssK head domain relative to the rest of
290 the trimer suggests that TssK may constitute a flexible link between the T6SS baseplate and
291 its membrane domain to accommodate the different conformations and radii before and after
292 tail contraction. The TssK flexible hinge would therefore prevent disruption of the contact
293 between the membrane and the baseplate complexes during sheath contraction.

294 By sharing the overall architecture and the N-terminal shoulder domain with RBPs, we
295 propose that TssK represents a RBP-like component of T6SS. Such as in RBPs, the TssK has
296 a modular architecture with a N-terminal shoulder domain and a C-terminal head domain.
297 The TssK shoulder domain interacts with the other T6SS baseplate components (TssFG). By
298 contrast, the head domain of TssK mediates interaction with the cytoplasmic domains of TssL
299 and TssM and hence docks the baseplate to the MC (Fig. 5). These data are consistent with
300 previous fluorescence microscopy imaging demonstrating that GFP-labeled TssK is recruited
301 to the MC and is necessary for recruiting the gp6/Mup47-like TssF baseplate subunit³⁴. Based
302 on these data and on the observation of TssE and TssG interactions with the cytoplasmic
303 domains of TssL and TssM respectively^{34,49,66}, we propose that TssK first interacts with the
304 MC and that TssE-TssL and TssG-TssL additional contacts stabilize the MC-BP complex.
305 TssK has therefore a similar function to RBPs: it is anchored to the phage-like structure by a
306 conserved shoulder domain but, instead of allowing the phage particle to bind to the target
307 cell surface, it has evolved a distinct head domain to recognize and bind to the T6SS MC. It
308 should be stressed that while TssFG have sequence similarity with *Myoviridae* phages
309 baseplate components, the TssK shoulder domain has structural similarity with *Siphoviridae*
310 phages RBPs, and has no counterpart in *Myoviridae*. Therefore, even if the origin of T6SS tail
311 and baseplate is from *Myoviridae* phages, the TssK N-terminal domain may derive from
312 horizontal transfer from a *Siphoviridae* component in order to provide the ability to bind the
313 TssJLM complex of T6SS). These results point to a more complicated evolutionary process
314 leading to the T6SS where elements of different phage types were combined.

315

316 **Materials and Methods**

317

318 *Bacterial strains, growth conditions and chemicals*

319 The strains used in this study are listed in Supplementary Table 3. *Escherichia coli* K-12
320 strains DH5 α , W3110, BTH101 and T7 Iq pLys were used for cloning procedures, co-
321 immune-precipitation, bacterial two-hybrid and protein purification respectively. The
322 enteroaggregative *E. coli* (EAEC) wild-type O3:H2 17-2 strain genomic DNA was used as
323 template for cloning. *E. coli* K-12 and EAEC cells were routinely grown in LB broth at 37°C,
324 with aeration. For protein production, cells were grown in terrific broth. Plasmids and
325 mutations were maintained by the addition of ampicillin (100 μ g/mL), kanamycin (50 μ g/mL)
326 or chloramphenicol (40 μ g/mL). Gene expression was induced by the addition of iso-propyl-
327 β -D-thio-galactopyranoside (IPTG, Sigma-Aldrich, 1 mM for nanobodies, 0.5 mM for TssK
328 and TssK domains production and BACTH analyses), L-arabinose (Sigma-Aldrich; 0.2%) or
329 anhydrotetracyclin (AHT; IBA Technologies; 0.2 μ g/mL).

330

331 *Plasmid construction*

332 PCR were performed with a Biometra thermocycler, using the Pfu Turbo DNA polymerase
333 (Stratagene; La Jolla, CA). Plasmids and oligonucleotides are listed in Supplementary Table
334 3. Plasmids producing EAEC TssK domains fused to a VSV-G tag or to the T18 or T25
335 domains of the *B. pertussis* adenylate cyclase were engineered by restriction-free cloning⁶⁷.
336 Briefly, DNA fragments corresponding to TssK domains were amplified from EAEC 17-2
337 genomic DNA using oligonucleotides bearing 5' extensions annealing on the target plasmid.
338 The PCR products were then used as primers for amplification of the target plasmid.
339 Constructs have been screened by colony-PCR and verified by DNA sequencing. The TssK_H
340 domain (residues S316 to T445) was cloned into the pETG20A expression vector using the
341 same procedure.

342 The *tssK*, *tssF* and *tssG* were initially cloned in a pCDF-Duet1 vector with Cter His₆tag, Nter
343 TREP tag and Cter FLAG tag for The *tssK*, *tssF* and *tssG*, respectively (Supplementary
344 Figure 8). For this study, the TREP and FLAG tags were removed by overlapping PCR
345 (Supplementary Figure 8). The *tssK_{SN}FG* and *tssK_HFG* vectors were obtained by Gibson
346 assembly (Gibson Assembly Cloning Kit, New England BioLabs) (Supplementary Figure 9).

347

348 *Bacterial two-hybrid*

349 The adenylate cyclase-based bacterial two-hybrid technique⁶⁸ was used as previously
350 published⁶⁹. Briefly, the proteins to be tested were fused to the isolated T18 and T25
351 catalytic domains of the *Bordetella* adenylate cyclase. After introduction of the two plasmids
352 producing the fusion proteins into the reporter BTH101 strain, plates were incubated at 30°C
353 for 24 hours. Three independent colonies for each transformation were inoculated into 600 µL
354 of LB medium supplemented with ampicillin, kanamycin and IPTG (0.5 mM). After
355 overnight growth at 30°C, 10 µL of each culture were dropped onto LB plates supplemented
356 with ampicillin, kanamycin, IPTG and 5-bromo-4-chloro-3-indolyl-β-D-galactopyranoside
357 (X-Gal) and incubated for 12 hours at 30 °C. Controls include interaction assays with TolB
358 and Pal, two protein partners unrelated to the T6SS. The experiments were done at least in
359 triplicate and a representative result is shown.

360 *Co-immunoprecipitation*

361 Co-immunoprecipitation experiments were performed as previously described³⁵. 10¹¹
362 exponentially growing cells producing the proteins of interest were harvested, and
363 resuspended in CellLytic™ B Cell Lysis reagent (Sigma-Aldrich) supplemented with protease
364 inhibitors (Complete, Roche), lysozyme (100 µg/mL) and DNase (100 µg/mL) and incubated

365 for 1 hour with strong shaking. The insoluble material was discarded by centrifugation for 45
366 min at $60,000\times g$ and the supernatant from 2×10^{10} cells was incubated overnight at 4°C with
367 anti-FLAG M2 affinity beads (Sigma-Aldrich). Beads were then washed twice with
368 CellLyticTM and once with Tris-HCl 20 mM pH8.0, NaCl 100 mM. The total extract and
369 immunoprecipitated material were resuspended and boiled in Laemmli loading buffer prior to
370 analyses by SDS-PAGE and immunoblotting.

371 *High-performance liquid size-exclusion chromatography*

372

373 Size exclusion chromatography was performed on an Ultimate 3000 HPLC system (Dionex),
374 using a Superdex 200 increase 10/30GL column equilibrated in Tris 10mM pH8, NaCl 150
375 mM at a flow rate of 0.6ml/min. Accurate injections of 30 ul samples were done using the
376 autosampler and detection was monitored at 280nm.

377

378 *Gel filtration analyses*

379 The effect of domains deletions on TssKFG as well as the binding of nanobodies nbK18 and
380 nbK27 to TssK_{SN}FG were analyzed using nickel affinity chromatography and gel filtration
381 chromatography. The three constructs possess a unique module bearing a His₆ tag
382 (Supplementary Figure 9): On TssK for the TssKFG construct, on TssK_H for the TssK_HFG
383 construct, and on TssK_{SN} for the TssK_{NS}FG construct. The purification procedures were
384 similar to those used for the TssK-nbK18 complex (see above). An molar excess of nanobody
385 (1.2), nbK18 or nbK25, was added to the TssK_{SN}FG complex and submitted to a nickel
386 affinity purification, followed by gel filtration. The mixtures were immobilized on a 5-mL
387 Ni²⁺ HisTrap prepacked column (GE Healthcare) using an AKTA FPLC system. After
388 extensive washing steps in absence or presence of 50 mM of imidazole, they were eluted with

389 250 mM imidazole. The fractions containing the His₆ tagged proteins were pooled and loaded
390 on to a preparative 10/300 Superdex 200 gel filtration column (GE Healthcare) equilibrated in
391 20 mM Tris-HCl, pH 8.0, 150 mM NaCl. The peaks were analysed by SDS gels. The same
392 conditions were applied to the TssK_HFG construct. The fractions containing the His₆ tagged
393 proteins were pooled and loaded on to aHiLoad 16/600 Superdex 200, column equilibrated in
394 20 mM Tris-HCl pH 8.0, 150 mM NaCl buffer.

395 *Protein purification.*

396 6×His-tagged TssK was purified as previously described⁴⁸. *E. coli* T7 Iq pLys cells carrying
397 pRSF-TssK (TssK_{6His}) or pETG20A-TssK_{Ct} (TssK C-terminal domain fused to a thioredoxin-
398 6×His-TEV N-terminal extension, TRX-6His-TEV-TssK_{Ct}) were grown at 37 °C in terrific
399 broth to an optimal optical density (OD₆₀₀) ~ 0.6-1.0 and *tssK* expression was induced with
400 0.5 mM IPTG for 16 h at 17 °C. Cells were harvested, resuspended in 50 mM Tris-HCl pH
401 8.0, 300 mM NaCl supplemented with 1 mM PMSF, 0.25 mg/mL lysozyme, 100 µg/mL
402 DNase I and 20 mM MgCl₂. After sonication, soluble proteins were separated from inclusion
403 bodies and cell debris by centrifugation at 20,000 × *g* for 30 min. TssK_{6His} and TRX-6His-
404 TEV-TssK_{Ct} were immobilized on a 5-mL Ni²⁺ HisTrap prepacked column (GE Healthcare)
405 using an AKTA FPLC system. After extensive washing steps in absence or presence of 50
406 mM of imidazole, TssK_{6His} and TRX-6His-TEV-TssK_{Ct} were eluted with 250 mM imidazole.
407 The fractions containing the TssK_{6His} protein were pooled and loaded on to a preparative
408 Superdex 200 gel filtration column (GE Healthcare) equilibrated in 20 mM Tris-HCl, pH 8.0,
409 150 mM NaCl. TssK_{6His} was concentrated to 25 mg/mL and stored at 4 °C for crystallization
410 trials. The fractions containing TRX-6His-TEV-TssK_{Ct} were pooled and incubated with TEV
411 protease (protein/TEV to a 20/1 molecular ratio) coupled to dialysis against 50 mM Tris-HCl
412 pH 8.0, 300 mM NaCl supplemented with 10 mM imidazole overnight at 4 °C. The proteins
413 were then subjected to a second Ni²⁺ HisTrap prepacked column. The untagged TssK_H protein

414 was collected in the flow through and concentrated on a preparative Superdex 200 gel
415 filtration column equilibrated in 20 mM Tris-HCl, pH 8.0, 150 mM NaCl. TssK_H was
416 concentrated to 26 mg/mL and stored at 4 °C for crystallization trials. pETG20A-TssK_{SN}
417 (TssK N-terminal domain fused to a thioredoxin-6×His-TEV N-terminal extension, TRX-
418 6His-TEV-TssK_{SN}) was prepared and purified in the same conditions as TssK_{6His}.

419

420 *Generation and purification of TssK-specific llama nanobodies.*

421 To obtain nanobodies against TssK, a llama (*Lama glama*) was immunized with
422 purified TssK_{6His} (Ardèche-lamas France). Approximately 400 µg of TssK_{6His} in 10 mM
423 HEPES, 150 mM NaCl, pH 7.5, was injected subcutaneously four times at one-week intervals
424 using incomplete Freund's adjuvant, followed by a fifth injection two weeks later. Blood
425 samples were collected aseptically 5 days after the last boost. Lymphocytes were isolated
426 from blood samples, and cDNA was synthesized from the acquired RNA using a reverse PCR
427 protocol. A nanobody phage display library of approximately 10⁹ independent transformants
428 was generated using the phagemid vector pHEN4^{70,71}. Phage display selection and screening
429 of specific nanobodies were performed as previously published⁷². An enrichment of antigen-
430 specific clones was observed after two consecutive rounds of selection on solid-phase coated
431 antigen. After the second round, TssK-specific nanobodies were identified, and the inserts of
432 the corresponding pHEN4-derived plasmids were sequenced and cloned into the pHEN6
433 vector. *E. coli* WK6 cells carrying the pHEN6 derivatives were grown at 37°C in terrific broth
434 supplemented with 0.1 % glucose and 100 µg/mL ampicillin to an optical density ~ 0.6-1.0
435 and the expression of the nanobodies was induced by the addition of 1 mM IPTG for 16 h at
436 28°C. The periplasmic fraction containing the nanobodies was prepared using mild osmotic
437 shock and the His-tagged nanobodies were immobilized on a 5-mL Ni-NTA column
438 equilibrated in 50 mM Tris-HCl, pH 8.0, 300 mM NaCl, and 10 mM imidazole. Nanobodies

439 were eluted in 250 mM imidazole and concentrated using the Amicon-technology (10-kDa
440 cut-off) prior to loading on a HiLoad 16/60 Superdex 75 gel filtration column equilibrated in
441 20 mM Tris-HCl, pH 8.0, 150 mM NaCl. The final concentration for NbK18 and NbK27
442 were 13 mg/mL and 10 mg/mL, respectively.

443

444 *Crystallization and structure determination of nbK18, TssK-nbK18 complex, TssK_H and*
445 *TssK_{SN}-nbK18-nbK27.*

446 Crystallization screening experiments were performed with several commercial kits, including
447 STURA, WIZARD and MDL. The nanodrop crystallization experiments were performed in
448 SWISSCI 3-well plates. The reservoirs of the SWISSCI plates were filled up using a TECAN
449 pipetting robot, while the nanodrops were dispensed with a Mosquito robot. All
450 crystallization experiments were performed at 293 K. For nbK18, a single crystal was
451 obtained by mixing 100 nL of the nbK18 protein solution with 100 nL of 0.2 M Li₂SO₄, 0.1
452 M NaAc, pH 4.75, and 30 % m/v PEG8000. The crystal was cryo-cooled in reservoir liquid
453 supplemented with 5 % ethylene glycol. For the TssK-nbK18 complex, purified TssK was
454 mixed with nbK18 (TssK:nbK18 at 1:1.2 molecular ratio), and then adjusted to a
455 concentration of 10 mg/mL for 1 hour prior to crystallization experiments. Small crystals
456 were obtained in 100 mM Tris-HCl, pH 8.5, 200 mM MgCl₂, 15 % PEG-6000. Optimization
457 was achieved by varying the concentration of PEG-6000 from 8 to 20 % m/v and the pH from
458 8 to 9. Quality crystals were obtained in 100 mM Tris-HCl, pH 8.3, 200 mM MgCl₂, 10 %
459 PEG-6000. All crystals, including CsI/NaI derivatives, were cryo-cooled in a well solution
460 supplemented with 20 % ethylene glycol. For the CsI/NaI derivatives, the TssK-nb18 crystals
461 were soaked for a few seconds in a well solution supplemented with 20 % ethylene glycol and
462 0.5 M CsI/NaI. For TssK_H, the best crystals appeared in 400 mM NaH₂PO₄, 1.6 M K₂HPO₄,
463 100 mM imidazole, pH 8.0. Crystals were flash cooled in 5 M sodium formate. Crystals of the

464 TssK_{SN}-nbK18-nbK27 complex were obtained in the STURA Footprint Screening plate.
465 TssK_{SN} (35 mg/ml) was mixed with the purified nanobodies nbK18 and nbK27 concentrations
466 of 10 mg/ml, with a molar excess of 1.2 vs TssK_{SN}. A volume of 100 nL of the proteins
467 mixtures was mixed with 45% PEG600, 0.1 M HEPES pH 7.5, and disposed over the
468 reservoir. Crystals appear in a few days. Crystals were cryo-cooled in the mother liquor.
469 Data collection was performed at ID23-2 (ESRF synchrotron, Grenoble, France) for nbK18
470 and TssK_H, and at Proxima 1 (Soleil synchrotron, Saint-Aubin, France) for the TssK-nbK18
471 complex and the data for the crystal of the TssK_{SN}-nbK18-nbK27 complex were collected at
472 ESRF beam line ID30A-3 (Supplementary Table 1). The data were integrated and scaled
473 with the XDS/XSCALE package and converted to a ccp4 input format file by XDSCONV⁷³.
474 For nbK18, the crystal diffracted up to 1.5 Å (Supplementary Table 1) and belonged to space
475 group P4₃, with cell dimensions a = b = 53.4 Å, c = 88.0 Å; $\alpha = \beta = \gamma = 90^\circ$. Two molecules
476 in the symmetric unit yielded a V_m value of 2.29 Å³/Da and 46.35 % solvent. Molecular
477 replacement was performed using MOLREP⁷⁴ and a truncated nanobody structure as a
478 starting model. Refinement was performed using autoBUSTER⁷⁵ alternating with rebuilding
479 with COOT⁷⁶. Two nbK18 molecules are contained in an asymmetric unit and possesses a
480 shorter complementary-determining region 3 (CDR3) compared to those usually found in
481 camelid single-chain domains. For TssK-nbK18, the crystal belonged to the orthorhombic
482 space group P2₁2₁2₁ with cell dimensions a=93.3, b=153.7, b=154.8 Å; $\alpha = \beta = \gamma = 90^\circ$.
483 Diffraction images were processed and scaled with the XDS/XSCALE package⁷³. The high-
484 resolution data cut-offs were defined based on the CC1/2 statistical indicator⁷⁷. Molecular
485 replacement on the native data set using the structure of nbK18 provided the positions of three
486 nbK18, but this did not yield a good enough initial electron density map. Therefore, three
487 360-degree rotation datasets were collected at different positions of the large single CsI/NaI
488 crystal derivative at 1.7712-Å X-ray wavelength to 3.5-Å resolution. The heavy atom

489 substructure, comprising 20 sites, was obtained with the SHELXC/D/E software suite⁷⁸ using
490 the HKL2MAP graphical interface⁷⁹. This sub-structure was subsequently refined and used
491 for phase calculation with PHASER⁸⁰. Phase improvement and extension by density
492 modification using 3-fold non-crystallographic symmetry averaging performed with
493 PARROT⁸¹ produced readily interpretable maps that allowed positioning of the three nbK18
494 and a first rough TssK model to be built. Inspection of electron density maps and model
495 adjustment and rebuilding were performed using COOT⁷⁶, and BUSTER was used for model
496 refinements⁷⁵. The initial refined model was then positioned by molecular replacement with
497 MOLREP⁷⁴ in a 2.7 Å resolution native dataset collected at 0.9786-Å wavelength with cell
498 dimensions a=93.3, b=153.7, c=154.8 Å. Then, several iterations of model improvement were
499 conducted by cycling through refinement with autoBUSTER⁷⁵, phase improvement by density
500 modification with PARROT⁸¹, auto-tracing with BUCCANEER⁸² and manual pruning and
501 rebuilding using COOT⁷⁶. The structure of TssK_H was obtained by molecular replacement
502 using MOLREP⁷⁴ using the partial structure in the refined full-length TssK and a 1.6-Å
503 resolution dataset. Refinement and manual building were performed as described above. The
504 TssK_{SN}-nbK18-nbK27 data were processed and scaled with the XDS/XSCALE package⁷³.
505 The crystals belong to the same space group as TssK-nbK18 (P2₁2₁2₁) with a comparable
506 packing and cell dimensions of a=90.9, b=143.3, c=150.3. The structure was determined by
507 molecular replacement with MOLREP⁷⁴ using the TssK_{SN} and nbK18 structures as separate
508 models. The resulting map made it possible to complete the missing segments of TssK_{SN} (1-
509 19 and 130-144) as well to construct the nbK27 model using alternate manual fitting with
510 COOT⁷⁶ and autoBUSTER⁷⁵ for model refinements at 2.2 Å resolution (Supplementary Table
511 1).

512

513 *Bilayer interferometry (BLI)*

514 NbK18 was biotinylated using the EZ-Link NHS-PEG4-Biotin kit (Perbio Science,
515 France). The reaction was stopped by removing the excess biotin reagent using a Zeba Spin
516 Desalting column (Perbio Science, France). BLI assays were performed in black 96-well
517 plates using an OctetRed96 (ForteBio, USA) apparatus. The total working volume for
518 samples or buffer was 0.2 ml and the rpm setting was 1000 rpm for baseline, loading, and
519 association and dissociation steps. The experiments were performed at 25°C. Prior to each
520 assay, streptavidin (SA) biosensor tips (ForteBio, USA) were hydrated in 0.2 ml kinetic
521 buffer (KB, ForteBio, USA) for 20 min. Streptavidin (SA) biosensor tips were then loaded
522 with biotinylated nbK18 at 5 mg/mL in KB, followed by a quenching step using biocytin. A
523 baseline was recorded, and nbK18 binding to TssK_{6His} was performed at concentrations of
524 0.08 to 50 nM. Association and dissociation were carried out for 300 s and 600 s,
525 respectively. Complete dissociation of the complex was achieved by three-fold regeneration
526 (5 s in glycine 10 mM, pH 1.7) and neutralization (5 s in KB).

527

528 **Data availability and accession codes**

529 Structures of nbK18, TssK-nbK18 complex, TssK_{SN}-nbK18-nbK27 complex and TssK_H were
530 deposited in the Protein Data Bank (PDB) under accession numbers 5M2W, 5M30, 5MWN
531 and 5M2Y, respectively.

532

533 **Author contributions**

534 V.S.N., E.C. and C.C. designed the study. V.S.N., L.L., S.S., P.L., T.T.H.P., T.T.N.T., Y.C.,
535 A.Z., A.D., E.D., A.R., C.K., E.C. and C.C. contributed to analysis of the data and
536 preparation of this manuscript. V.S.N., S.S., P.L. and C.C. perform the proteins production,
537 crystallization and crystallographic experiments. T.T.H.P. and T.T.N.T. contributed to protein

538 production and crystallization. A.D. performed the nanobodies selection and characterization.
539 E.D. provided the TssKFG clone. C.K. performed the BLI and HPLC experiments. L.L.,
540 Y.C., A.Z. and E.C performed the double hybrid and co-immunoprecipitation experiments.
541

542 **Funding information**

543 This work was supported by the Centre National de la Recherche Scientifique and the Aix-
544 Marseille Université, and grants from the Agence Nationale de la Recherche (ANR-14-CE14-
545 0006-02) and the French Infrastructure for Integrated Structural Biology (FRISBI). V.S.N
546 was supported by a fellowship from the French Embassy in Vietnam. L.L. and A.Z. were
547 supported by doctoral fellowships of the Ministère Français de l'Enseignement Supérieur et de
548 la Recherche and end-of-thesis fellowships from the Fondation pour la Recherche Médicale
549 (FRM) (FDT20160435498 and FDT20140931060 respectively). T.T.N.T. was supported by a
550 grant from the Ministère des Affaires Etrangères – France (N°861733C). Y.C. is supported by
551 a doctoral school PhD fellowship from the FRM (ECO20160736014).

552

553 **Correspondence and requests for materials** should be addressed to E.C. and C.C.

554

555 **Acknowledgements**

556 We thank the members of the Cambillau/Roussel and Cascales laboratories for insightful
557 discussions, Amel Kassa for initial work on TssK, Laure Journet for critical reading of the
558 manuscript, the Soleil (Saint Aubin, France) and ESRF (Grenoble, France) synchrotrons for
559 beam time allocation and Annick Brun, Isabelle Bringer and Olivier Uderso for technical
560 assistance.

561

562 **References**

- 563 1 Costa, T. R. *et al.* Secretion systems in Gram-negative bacteria: structural and
564 mechanistic insights. *Nature reviews. Microbiology* **13**, 343-359,
565 doi:10.1038/nrmicro3456 (2015).
- 566 2 Bonemann, G., Pietrosiuk, A. & Mogk, A. Tubules and donuts: a type VI secretion
567 story. *Molecular microbiology* **76**, 815-821, doi:10.1111/j.1365-2958.2010.07171.x
568 (2010).
- 569 3 Cascales, E. & Cambillau, C. Structural biology of type VI secretion systems.
570 *Philosophical transactions of the Royal Society of London. Series B, Biological*
571 *sciences* **367**, 1102-1111, doi:10.1098/rstb.2011.0209 (2012).
- 572 4 Kapitein, N. & Mogk, A. Deadly syringes: type VI secretion system activities in
573 pathogenicity and interbacterial competition. *Current opinion in microbiology* **16**, 52-
574 58, doi:10.1016/j.mib.2012.11.009 (2013).
- 575 5 Zoued, A. *et al.* Architecture and assembly of the Type VI secretion system.
576 *Biochimica et biophysica acta* **1843**, 1664-1673, doi:10.1016/j.bbamcr.2014.03.018
577 (2014).
- 578 6 Ho, B. T., Dong, T. G. & Mekalanos, J. J. A View to a Kill: The Bacterial Type VI
579 Secretion System. *Cell host & microbe* **15**, 9-21, doi:10.1016/j.chom.2013.11.008
580 (2014).
- 581 7 Basler, M. Type VI secretion system: secretion by a contractile nanomachine.
582 *Philosophical transactions of the Royal Society of London. Series B, Biological*
583 *sciences* **370**, doi:10.1098/rstb.2015.0021 (2015).
- 584 8 Durand, E., Cambillau, C., Cascales, E. & Journet, L. VgrG, Tae, Tle, and beyond: the
585 versatile arsenal of Type VI secretion effectors. *Trends in microbiology* **22**, 498-507,
586 doi:10.1016/j.tim.2014.06.004 (2014).

- 587 9 Russell, A. B., Peterson, S. B. & Mougous, J. D. Type VI secretion system effectors:
588 poisons with a purpose. *Nature reviews. Microbiology* **12**, 137-148,
589 doi:10.1038/nrmicro3185 (2014).
- 590 10 Kapitein, N. & Mogk, A. Type VI secretion system helps find a niche. *Cell host &*
591 *microbe* **16**, 5-6, doi:10.1016/j.chom.2014.06.012 (2014).
- 592 11 Wexler, A. G. *et al.* Human symbionts inject and neutralize antibacterial toxins to
593 persist in the gut. *Proceedings of the National Academy of Sciences of the United*
594 *States of America* **113**, 3639-3644, doi:10.1073/pnas.1525637113 (2016).
- 595 12 Chatzidaki-Livanis, M., Geva-Zatorsky, N. & Comstock, L. E. Bacteroides fragilis
596 type VI secretion systems use novel effector and immunity proteins to antagonize
597 human gut Bacteroidales species. *Proceedings of the National Academy of Sciences of*
598 *the United States of America* **113**, 3627-3632, doi:10.1073/pnas.1522510113 (2016).
- 599 13 Sana, T. G. *et al.* Salmonella Typhimurium utilizes a T6SS-mediated antibacterial
600 weapon to establish in the host gut. *Proceedings of the National Academy of Sciences*
601 *of the United States of America* **113**, E5044-5051, doi:10.1073/pnas.1608858113
602 (2016).
- 603 14 Hecht, A. L. *et al.* Strain competition restricts colonization of an enteric pathogen and
604 prevents colitis. *EMBO reports* **17**, 1281-1291, doi:10.15252/embr.201642282 (2016).
- 605 15 Fu, Y., Waldor, M. K. & Mekalanos, J. J. Tn-Seq analysis of Vibrio cholerae intestinal
606 colonization reveals a role for T6SS-mediated antibacterial activity in the host. *Cell*
607 *host & microbe* **14**, 652-663, doi:10.1016/j.chom.2013.11.001 (2013).
- 608 16 Ma, L. S., Hachani, A., Lin, J. S., Filloux, A. & Lai, E. M. Agrobacterium tumefaciens
609 deploys a superfamily of type VI secretion DNase effectors as weapons for
610 interbacterial competition in planta. *Cell host & microbe* **16**, 94-104,
611 doi:10.1016/j.chom.2014.06.002 (2014).

- 612 17 Coulthurst, S. J. The Type VI secretion system - a widespread and versatile cell
613 targeting system. *Research in microbiology* **164**, 640-654,
614 doi:10.1016/j.resmic.2013.03.017 (2013).
- 615 18 Bingle, L. E., Bailey, C. M. & Pallen, M. J. Type VI secretion: a beginner's guide.
616 *Current opinion in microbiology* **11**, 3-8, doi:S1369-5274(08)00007-6 (2008).
- 617 19 Cascales, E. The type VI secretion toolkit. *EMBO reports* **9**, 735-741,
618 doi:10.1038/embor.2008.131 (2008).
- 619 20 Aschtgen, M. S., Bernard, C. S., De Bentzmann, S., Lloubes, R. & Cascales, E. SciN
620 is an outer membrane lipoprotein required for type VI secretion in enteroaggregative
621 Escherichia coli. *Journal of bacteriology* **190**, 7523-7531, doi:10.1128/JB.00945-08
622 (2008).
- 623 21 Aschtgen, M. S., Gavioli, M., Dessen, A., Lloubes, R. & Cascales, E. The SciZ
624 protein anchors the enteroaggregative Escherichia coli Type VI secretion system to the
625 cell wall. *Molecular microbiology*, doi:10.1111/j.1365-2958.2010.07028.x (2010).
- 626 22 Ma, L. S., Lin, J. S. & Lai, E. M. An IcmF family protein, ImpLM, is an integral inner
627 membrane protein interacting with ImpKL, and its walker a motif is required for type
628 VI secretion system-mediated Hcp secretion in Agrobacterium tumefaciens. *Journal of*
629 *bacteriology* **191**, 4316-4329, doi:10.1128/JB.00029-09 (2009).
- 630 23 Felisberto-Rodrigues, C. *et al.* Towards a structural comprehension of bacterial type
631 VI secretion systems: characterization of the TssJ-TssM complex of an Escherichia
632 coli pathovar. *PLoS pathogens* **7**, e1002386, doi:10.1371/journal.ppat.1002386
633 (2011).
- 634 24 Aschtgen, M. S., Zoued, A., Lloubes, R., Journet, L. & Cascales, E. The C-tail
635 anchored TssL subunit, an essential protein of the enteroaggregative Escherichia coli

- 636 Sci-1 Type VI secretion system, is inserted by YidC. *MicrobiologyOpen* **1**, 71-82,
637 doi:10.1002/mbo3.9 (2012).
- 638 25 Durand, E. *et al.* Structural characterization and oligomerization of the TssL protein, a
639 component shared by bacterial type VI and type IVb secretion systems. *The Journal of*
640 *biological chemistry* **287**, 14157-14168, doi:10.1074/jbc.M111.338731 (2012).
- 641 26 Durand, E. *et al.* Biogenesis and structure of a type VI secretion membrane core
642 complex. *Nature* **523**, 555-560, doi:10.1038/nature14667 (2015).
- 643 27 Aschtgen, M. S., Thomas, M. S. & Cascales, E. Anchoring the type VI secretion
644 system to the peptidoglycan: TssL, TagL, TagP... what else? *Virulence* **1**, 535-540
645 (2010).
- 646 28 Weber, B. S. *et al.* Genetic Dissection of the Type VI Secretion System in
647 *Acinetobacter* and Identification of a Novel Peptidoglycan Hydrolase, TagX, Required
648 for Its Biogenesis. *mBio* **7**, doi:10.1128/mBio.01253-16 (2016).
- 649 29 Santin, Y. G. & Cascales, E. Domestication of a housekeeping transglycosylase for
650 assembly of a Type VI secretion system. *EMBO reports* **18**, 138-149,
651 doi:10.15252/embr.201643206 (2017).
- 652 30 Leiman, P. G. *et al.* Type VI secretion apparatus and phage tail-associated protein
653 complexes share a common evolutionary origin. *Proceedings of the National Academy*
654 *of Sciences of the United States of America* **106**, 4154-4159,
655 doi:10.1073/pnas.0813360106 (2009).
- 656 31 Brunet, Y. R., Henin, J., Celia, H. & Cascales, E. Type VI secretion and bacteriophage
657 tail tubes share a common assembly pathway. *EMBO reports*,
658 doi:10.1002/embr.201337936 (2014).
- 659 32 Kudryashev, M. *et al.* Structure of the type VI secretion system contractile sheath.
660 *Cell* **160**, 952-962, doi:10.1016/j.cell.2015.01.037 (2015).

- 661 33 English, G., Byron, O., Cianfanelli, F. R., Prescott, A. R. & Coulthurst, S. J.
662 Biochemical analysis of TssK, a core component of the bacterial Type VI secretion
663 system, reveals distinct oligomeric states of TssK and identifies a TssK-TssFG sub-
664 complex. *The Biochemical journal*, doi:10.1042/BJ20131426 (2014).
- 665 34 Brunet, Y. R., Zoued, A., Boyer, F., Douzi, B. & Cascales, E. The Type VI Secretion
666 TssEFGK-VgrG Phage-Like Baseplate Is Recruited to the TssJLM Membrane
667 Complex via Multiple Contacts and Serves As Assembly Platform for Tail
668 Tube/Sheath Polymerization. *PLoS genetics* **11**, e1005545,
669 doi:10.1371/journal.pgen.1005545 (2015).
- 670 35 Zoued, A. *et al.* Priming and polymerization of a bacterial contractile tail structure.
671 *Nature* **531**, 59-63, doi:10.1038/nature17182 (2016).
- 672 36 Boyer, F., Fichant, G., Berthod, J., Vandembrouck, Y. & Attree, I. Dissecting the
673 bacterial type VI secretion system by a genome wide in silico analysis: what can be
674 learned from available microbial genomic resources? *BMC genomics* **10**, 104,
675 doi:10.1186/1471-2164-10-104 (2009).
- 676 37 Pell, L. G., Kanelis, V., Donaldson, L. W., Howell, P. L. & Davidson, A. R. The
677 phage lambda major tail protein structure reveals a common evolution for long-tailed
678 phages and the type VI bacterial secretion system. *Proceedings of the National*
679 *Academy of Sciences of the United States of America* **106**, 4160-4165,
680 doi:0900044106 (2009).
- 681 38 Kube, S. *et al.* Structure of the VipA/B type VI secretion complex suggests a
682 contraction-state-specific recycling mechanism. *Cell reports* **8**, 20-30,
683 doi:10.1016/j.celrep.2014.05.034 (2014).

- 684 39 Basler, M., Pilhofer, M., Henderson, G. P., Jensen, G. J. & Mekalanos, J. J. Type VI
685 secretion requires a dynamic contractile phage tail-like structure. *Nature* **483**, 182-
686 186, doi:10.1038/nature10846 (2012).
- 687 40 LeRoux, M. *et al.* Quantitative single-cell characterization of bacterial interactions
688 reveals type VI secretion is a double-edged sword. *Proceedings of the National*
689 *Academy of Sciences of the United States of America* **109**, 19804-19809,
690 doi:10.1073/pnas.1213963109 (2012).
- 691 41 Basler, M., Ho, B. T. & Mekalanos, J. J. Tit-for-tat: type VI secretion system
692 counterattack during bacterial cell-cell interactions. *Cell* **152**, 884-894,
693 doi:10.1016/j.cell.2013.01.042 (2013).
- 694 42 Brunet, Y. R., Espinosa, L., Harchouni, S., Mignot, T. & Cascales, E. Imaging type VI
695 secretion-mediated bacterial killing. *Cell reports* **3**, 36-41,
696 doi:10.1016/j.celrep.2012.11.027 (2013).
- 697 43 Lossi, N. S., Dajani, R., Freemont, P. & Filloux, A. Structure-function analysis of
698 HsiF, a gp25-like component of the type VI secretion system, in *Pseudomonas*
699 *aeruginosa*. *Microbiology* **157**, 3292-3305, doi:10.1099/mic.0.051987-0 (2011).
- 700 44 Planamente, S. *et al.* TssA forms a gp6-like ring attached to the type VI secretion
701 sheath. *The EMBO journal* **35**, 1613-1627, doi:10.15252/emj.201694024 (2016).
- 702 45 Taylor, N. M. *et al.* Structure of the T4 baseplate and its function in triggering sheath
703 contraction. *Nature* **533**, 346-352, doi:10.1038/nature17971 (2016).
- 704 46 Leiman, P. G. *et al.* Morphogenesis of the T4 tail and tail fibers. *Virology journal* **7**,
705 355, doi:10.1186/1743-422X-7-355 (2010).
- 706 47 Leiman, P. G. & Shneider, M. M. Contractile tail machines of bacteriophages.
707 *Advances in experimental medicine and biology* **726**, 93-114, doi:10.1007/978-1-
708 4614-0980-9_5 (2012).

709 48 Zoued, A. *et al.* TssK is a trimeric cytoplasmic protein interacting with components of
710 both phage-like and membrane anchoring complexes of the Type VI secretion system.
711 *The Journal of biological chemistry* **288** 27031–27041, doi:10.1074/jbc.M113.499772
712 (2013).

713 49 Logger, L., Aschtgen, M. S., Guerin, M., Cascales, E. & Durand, E. Molecular
714 Dissection of the Interface between the Type VI Secretion TssM Cytoplasmic Domain
715 and the TssG Baseplate Component. *J Mol Biol* **428**, 4424-4437,
716 doi:10.1016/j.jmb.2016.08.032 (2016).

717 50 Desmyter, A., Spinelli, S., Roussel, A. and Cambillau, C. Camelid nanobodies: killing
718 two birds with one stone. *Curr. Opin. Struct. Biol.* **32** 1-8 (2015).

719 51 Nguyen, V. S. *et al.* Inhibition of type VI secretion by an anti-TssM llama nanobody.
720 *PloS one* **10**, e0122187, doi:10.1371/journal.pone.0122187 (2015).

721 52 Nguyen, V. S. *et al.* Production, crystallization and X-ray diffraction analysis of a
722 complex between a fragment of the TssM T6SS protein and a camelid nanobody. *Acta*
723 *crystallographica. Section F, Structural biology communications* **71**, 266-271,
724 doi:10.1107/S2053230X15000709 (2015).

725 53 Desmyter, A. *et al.* Three Camelid VHH domains in complex with porcine pancreatic
726 alpha-amylase - Inhibition and versatility of binding topology. *Journal of Biological*
727 *Chemistry* **277**, 23645-23650, doi:10.1074/jbc.M202327200 (2002).

728 54 Spinelli, S., Tegoni, M., Frenken, L., van Vliet, C. & Cambillau, C. Lateral
729 recognition of a dye hapten by a llama VHH domain. *J Mol Biol* **311**, 123-129,
730 doi:10.1006/jmbi.2001.4856 (2001).

731 55 Drozdetskiy, A., Cole, C., Procter, J. & Barton, G. J. JPred4: a protein secondary
732 structure prediction server. *Nucleic acids research* **43**, W389-394,
733 doi:10.1093/nar/gkv332 (2015).

734 56 Pettersen, E. F. *et al.* UCSF Chimera--a visualization system for exploratory research
735 and analysis. *J Comput Chem* **25**, 1605-1612, doi:10.1002/jcc.20084 (2004).

736 57 Farenc, C. *et al.* Molecular insights on the recognition of a *Lactococcus lactis* cell wall
737 pellicle by phage 1358 receptor binding protein. *Journal of virology*,
738 doi:10.1128/JVI.00739-14 (2014).

739 58 Spinelli, S. *et al.* Lactococcal bacteriophage p2 receptor-binding protein structure
740 suggests a common ancestor gene with bacterial and mammalian viruses. *Nature*
741 *structural & molecular biology* **13**, 85-89, doi:nsmb1029 (2006).

742 59 Ray, S. P. *et al.* Structural and biochemical characterization of human
743 adenylosuccinate lyase (ADSL) and the R303C ADSL deficiency-associated mutation.
744 *Biochemistry* **51**, 6701-6713, doi:10.1021/bi300796y (2012).

745 60 Casabona, M. G., Vandenbrouck, Y., Attree, I. & Coute, Y. Proteomic
746 characterization of *Pseudomonas aeruginosa* PAO1 inner membrane. *Proteomics* **13**,
747 2419-2423, doi:10.1002/pmic.201200565 (2013).

748 61 Buttner, C. R., Wu, Y., Maxwell, K. L. & Davidson, A. R. Baseplate assembly of
749 phage Mu: Defining the conserved core components of contractile-tailed phages and
750 related bacterial systems. *Proceedings of the National Academy of Sciences of the*
751 *United States of America* **113**, 10174-10179, doi:10.1073/pnas.1607966113 (2016).

752 62 Spinelli, S. *et al.* Modular structure of the receptor binding proteins of *Lactococcus*
753 *lactis* phages. The RBP structure of the temperate phage TP901-1. *The Journal of*
754 *biological chemistry* **281**, 14256-14262 (2006).

755 63 Casjens, S. R. & Molineux, I. J. Short noncontractile tail machines: adsorption and
756 DNA delivery by podoviruses. *Advances in experimental medicine and biology* **726**,
757 143-179, doi:10.1007/978-1-4614-0980-9_7 (2012).

- 758 64 Spinelli, S., Veessler, D., Bebeacua, C. & Cambillau, C. Structures and host-adhesion
759 mechanisms of lactococcal siphophages. *Frontiers in microbiology* **5**, 3,
760 doi:10.3389/fmicb.2014.00003 (2014).
- 761 65 Sciara, G. *et al.* Structure of lactococcal phage p2 baseplate and its mechanism of
762 activation. *Proceedings of the National Academy of Sciences of the United States of*
763 *America* **107**, 6852-6857, doi:1000232107 (2010).
- 764 66 Zoued, A. *et al.* Structure-Function Analysis of the TssL Cytoplasmic Domain
765 Reveals a New Interaction between the Type VI Secretion Baseplate and Membrane
766 Complexes. *J Mol Biol* **428**, 4413-4423, doi:10.1016/j.jmb.2016.08.030 (2016).
- 767 67 van den Ent, F. & Lowe, J. RF cloning: a restriction-free method for inserting target
768 genes into plasmids. *Journal of biochemical and biophysical methods* **67**, 67-74,
769 doi:10.1016/j.jbbm.2005.12.008 (2006).
- 770 68 Karimova, G., Pidoux, J., Ullmann, A. & Ladant, D. A bacterial two-hybrid system
771 based on a reconstituted signal transduction pathway. *Proceedings of the National*
772 *Academy of Sciences of the United States of America* **95**, 5752-5756 (1998).
- 773 69 Battesti, A. & Bouveret, E. The bacterial two-hybrid system based on adenylate
774 cyclase reconstitution in *Escherichia coli*. *Methods* **58**, 325-334,
775 doi:10.1016/j.ymeth.2012.07.018 (2012).
- 776 70 Pardon, E. *et al.* A general protocol for the generation of Nanobodies for structural
777 biology. *Nature protocols* **9**, 674-693, doi:10.1038/nprot.2014.039 (2014).
- 778 71 Arbabi Ghahroudi, M., Desmyter, A., Wyns, L., Hamers, R. & Muyldermans, S.
779 Selection and identification of single domain antibody fragments from camel heavy-
780 chain antibodies. *FEBS letters* **414**, 521-526 (1997).

781 72 Desmyter, A. *et al.* Viral infection modulation and neutralization by camelid
782 nanobodies. *Proceedings of the National Academy of Sciences of the United States of*
783 *America* **110**, E1371-1379, doi:10.1073/pnas.1301336110 (2013).

784 73 Kabsch, W. Xds. *Acta Crystallogr D Biol Crystallogr* **66**, 125-132,
785 doi:S0907444909047337 (2010).

786 74 Vagin, A. & Teplyakov, A. Molecular replacement with MOLREP. *Acta Crystallogr*
787 *D Biol Crystallogr* **66**, 22-25, doi:10.1107/S0907444909042589 (2010).

788 75 Blanc, E. *et al.* Refinement of severely incomplete structures with maximum
789 likelihood in BUSTER-TNT. *Acta Crystallogr D Biol Crystallogr* **60**, 2210-2221,
790 doi:S0907444904016427 (2004).

791 76 Emsley, P., Lohkamp, B., Scott, W. G. & Cowtan, K. Features and development of
792 Coot. *Acta Crystallogr D Biol Crystallogr* **66**, 486-501,
793 doi:10.1107/S0907444910007493 (2010).

794 77 Karplus, P. A. & Diederichs, K. Linking crystallographic model and data quality.
795 *Science* **336**, 1030-1033, doi:10.1126/science.1218231 (2012).

796 78 Sheldrick, G. M. A short history of SHELX. *Acta Crystallogr A* **64**, 112-122,
797 doi:10.1107/S0108767307043930 (2008).

798 79 Pape, T. a. S., T.R. HKL2MAP: a graphical user interface for macromolecular phasing
799 with SHELX programs. *J. Applied Crystallogr.* **37**, 853-844 (2004).

800 80 McCoy, A. J. *et al.* Phaser crystallographic software. *Journal of applied*
801 *crystallography* **40**, 658-674, doi:10.1107/S0021889807021206 (2007).

802 81 Cowtan, K. Recent developments in classical density modification. *Acta Crystallogr D*
803 *Biol Crystallogr* **66**, 470-478, doi:10.1107/S090744490903947X (2010).

804 82 Cowtan, K. The Buccaneer software for automated model building. 1. Tracing protein
805 chains. *Acta Crystallogr D Biol Crystallogr* **62**, 1002-1011,
806 doi:10.1107/S0907444906022116 (2006).

807

808 **Legend to Figures**

809

810 **Figure 1. Structure of TssK.** **a**, Ribbon view of the TssK trimer. Monomers A, B and C are
811 colored pink, blue and green, respectively. The location of the N-terminal (shoulder), central
812 (neck) and C-terminal (head) domains is indicated. **b**, Ribbon view of TssK monomer B (full-
813 length TssK). The monomer is rainbow-colored (blue to red from N- to C-terminal). The α -
814 helices and β -strands are numbered. **(c, d)** Side **(c)** and bottom **(d)** views of the TssK X-ray
815 structure fitted into the TssK negative-stain electron microscopy map (EMD-5739),
816 highlighting that the TssK C-terminal head domain is disordered.

817

818 **Figure 2. Structure of the TssK_{SN}-nbK18-nbK27 complex.** **a**, Ribbon view of the TssK_{SN}-
819 nbK18-nbK27 complex. Monomers A, B and C are colored pink, blue and green,
820 respectively. The three nbK18 are colored grey and the unique nbK27 is colored beige. **b**,
821 Same view as in **(a)**, rotated by 90° presenting the bottom of the TssK_{SN} domain. **c**, Same
822 orientation and colors as in **(b)**, but with a molecular surface representation. **d**, Same
823 orientation as in **(b)**. The TssK_{SN} domain trimer (beige) and the nbK18 nanobody (grey) are
824 represented as ribbons. The TssK_{SN} N-terminal segments ordered upon surface binding are
825 identified by their ribbon darker color (brown) and their green semi-transparent surface.

826

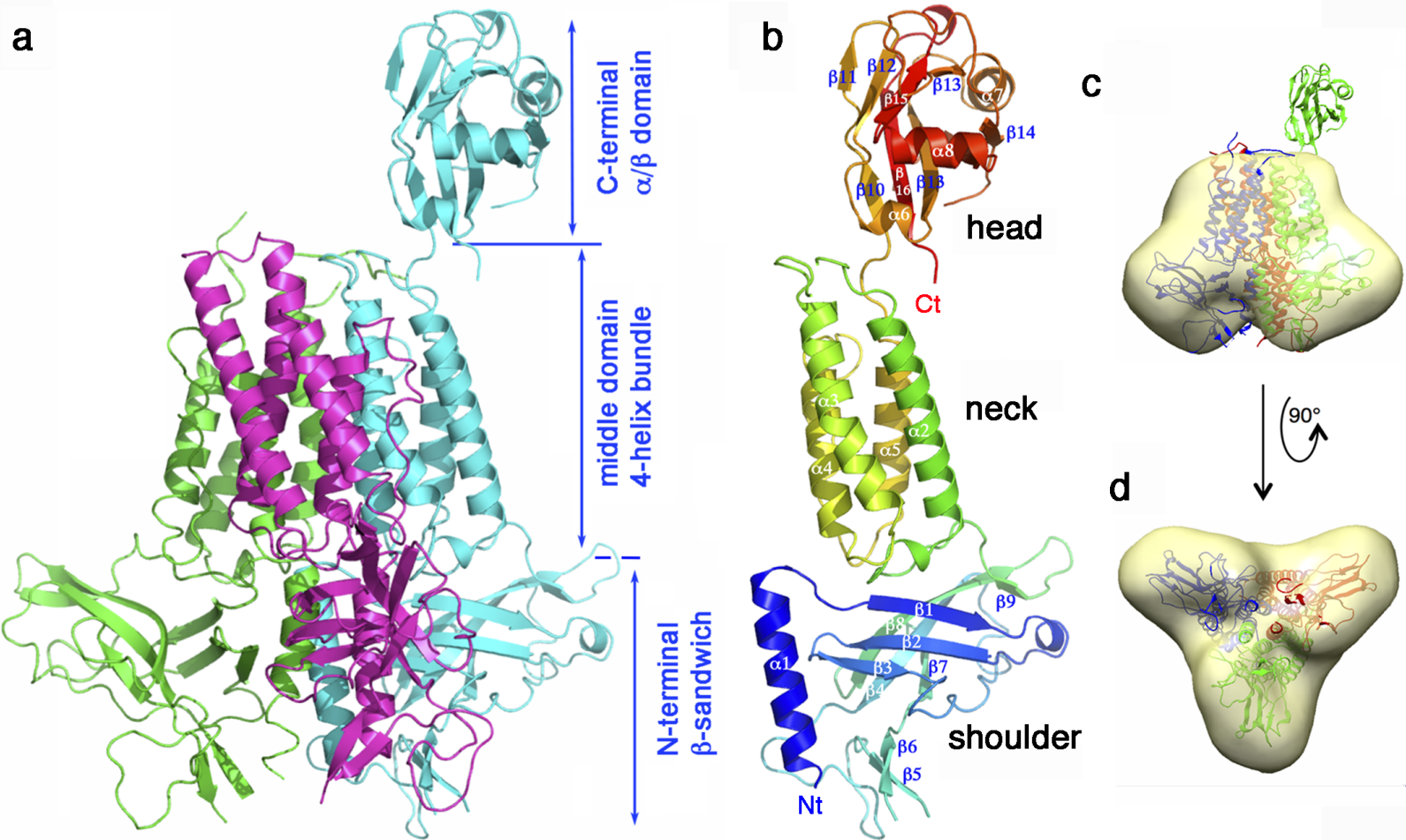
827 **Figure 3. Structural comparison of the TssK N-terminal shoulder domain with shoulder**
828 **domains of siphophage receptor-binding proteins.** Superimposed ribbon views of the TssK
829 N-terminal shoulder domain (pink) with the shoulder domains of phages p2 (green) and 1358
830 (blue) RBPs (PDB 1ZRU and 4L9B respectively).

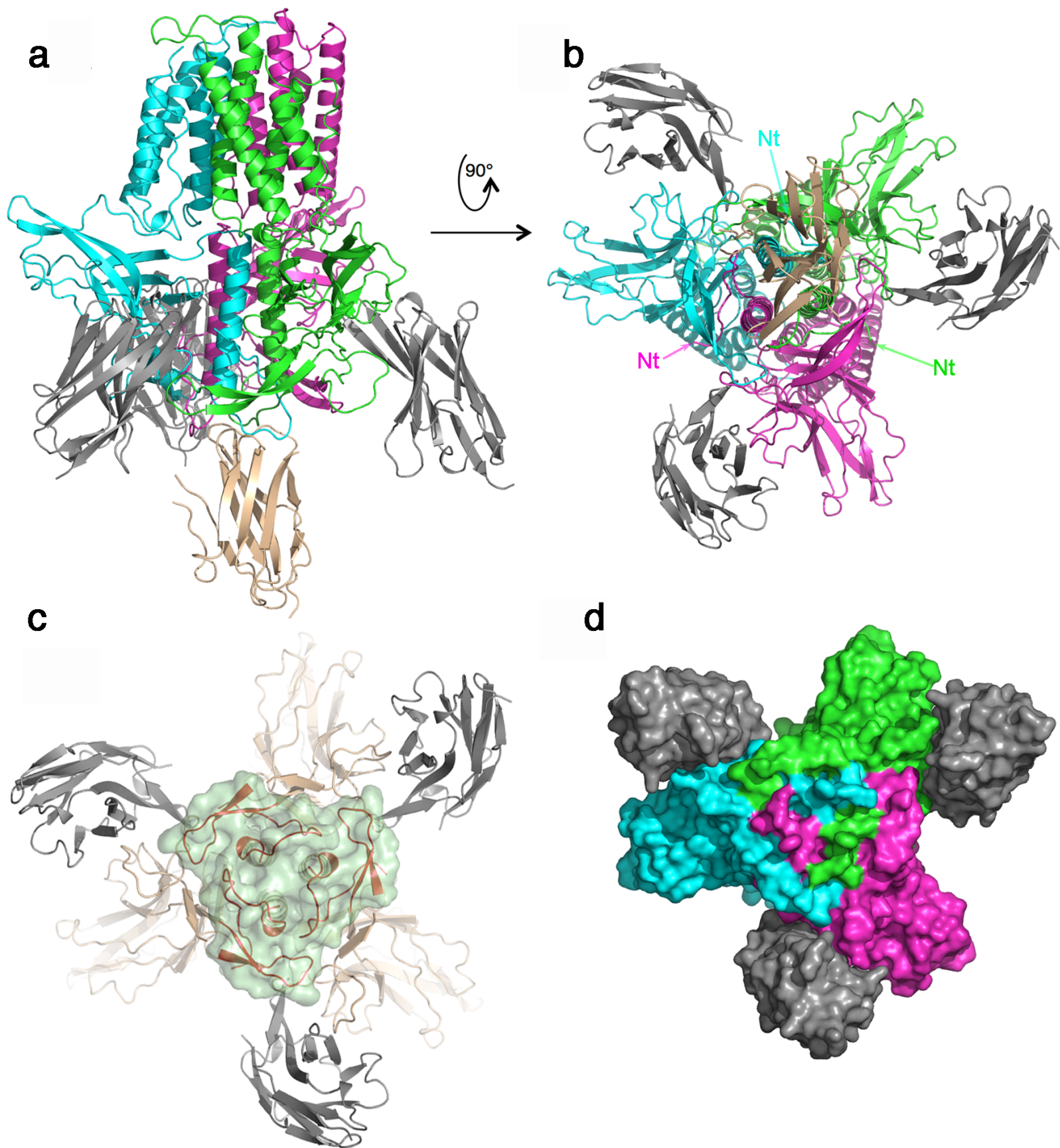
831

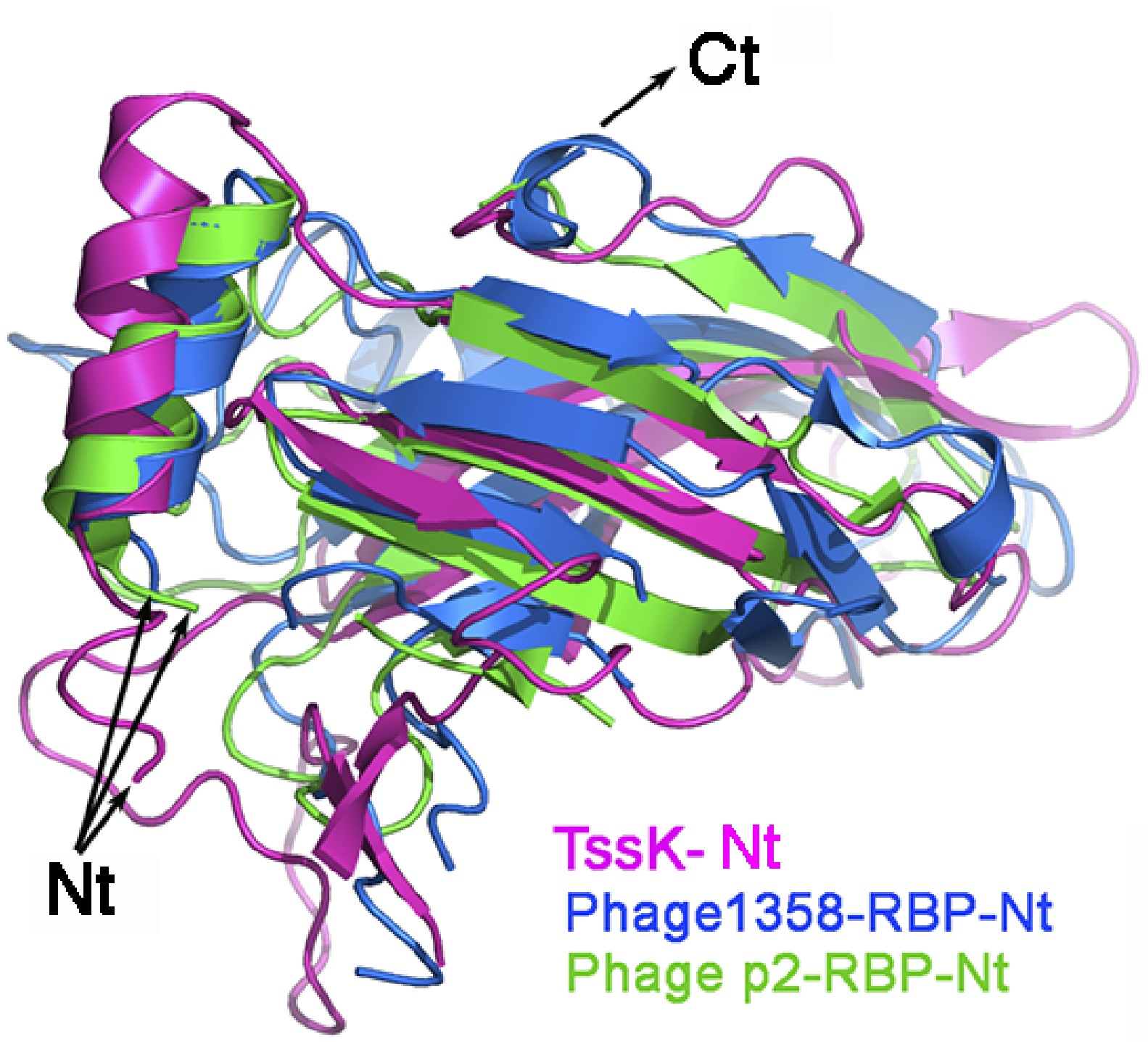
832 **Figure 4. Protein-protein interaction study of TssK domains. a,** Bacterial two-hybrid
833 assay. BTH101 reporter cells producing the indicated proteins or domains (K, TssK; K_{SN},
834 TssK shoulder and neck domains; K_S, TssK shoulder domain; K_N, TssK neck domain; K_H,
835 TssK head domain) fused to the T18 or T25 domain of the Bordetella adenylate cyclase were
836 spotted on X-Gal indicator plates. The blue color of the colony reflects the interaction
837 between the two proteins. TolB and Pal are two proteins known to interact but unrelated to the
838 T6SS. The BACTH experiments have been performed in triplicate with identical results. **b,**
839 Co-immunoprecipitation assay. A mixture of soluble lysates from 2×10^{10} *E. coli* K-12
840 W3110 cells producing VSV-G-tagged TssK shoulder + neck (K_{SN}), TssK shoulder (K_S) and
841 TssK head (K_H) domains (individually shown on the left panel) was mixed with FLAG-
842 tagged TssF + TssG, TssL_C or TssM_C. FLAG-tagged proteins were subjected to
843 immunoprecipitation with anti-FLAG-coupled beads, and the immunoprecipitated material
844 was separated by 12.5% crylamide SDS-PAGE and immunodetected anti-VSV-G monoclonal
845 antibodies. The position of each protein and domain is indicated, Molecular weight markers
846 (in kDa) are indicated on the right. The co-immunoprecipitation experiments have been
847 performed in duplicate with identical results. **c,** Gel filtration chromatograms of TssKFG
848 (brown), TssK_{SN}FG (red), TssK_{SN}FG + nbK18 (blue) and TssK_{SN}FG + nbK27 (green); **inset:**
849 enlargement of the top of the peaks; the elution time is indicated above each peak. **d,** SDS gels
850 of the main peak of TssKFG (brown) and TssK_{SN}FG (red) showing the presence of TssK,
851 TssF and TssG, and TssK_{SN}, TssF and TssG, respectively. **e,** SDS gels of the main peak of
852 TssK_{SN}FG (red), TssK_{SN}FG + nbK18 (blue) and TssK_{SN}FG + nbK27 (green) showing the
853 presence of nbK18 attached to TssK_{SN}FG, but not nbK27. **a-b:** The experiments were done
854 at least in triplicate and a representative result is shown. **c-e:** The experiments were done in
855 triplicate and a representative result is shown.

856

857 **Figure 5. Schematic model of the baseplate docked to the membrane complex,**
858 **highlighting the connector role of TssK.** The TssJLM membrane complex is represented in
859 green whereas TssK is colored beige and the other baseplate components, TssFGE are colored
860 blue, VgrG is yellow and Hcp orange. The tail complex is shown in dark green. The three
861 domains of TssK are represented in beige, the N-terminal shoulder domain anchored to the
862 baseplate and the C-terminal head domain bound to the membrane complex.



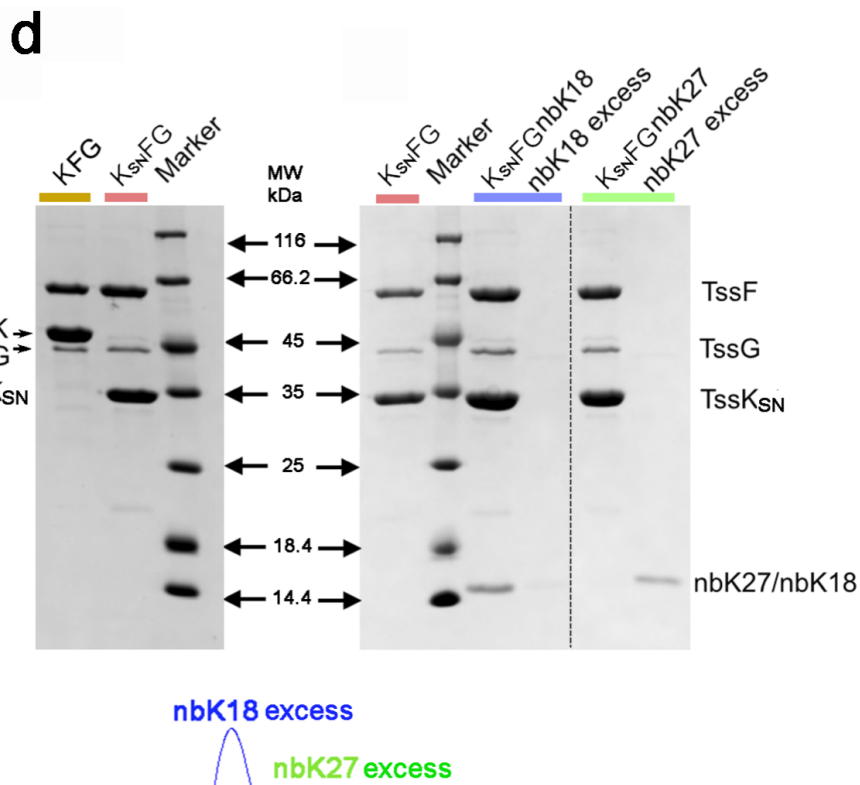
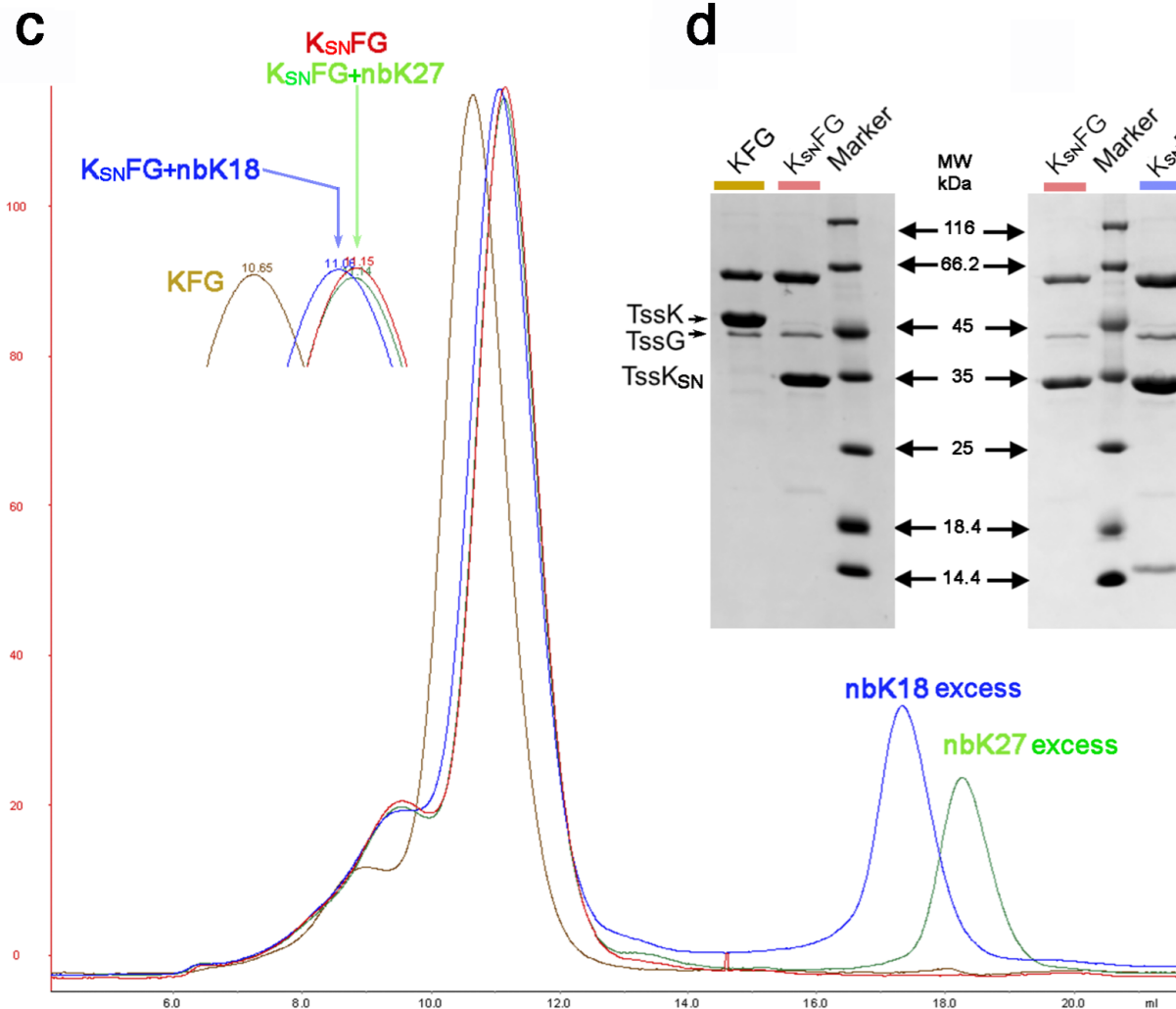
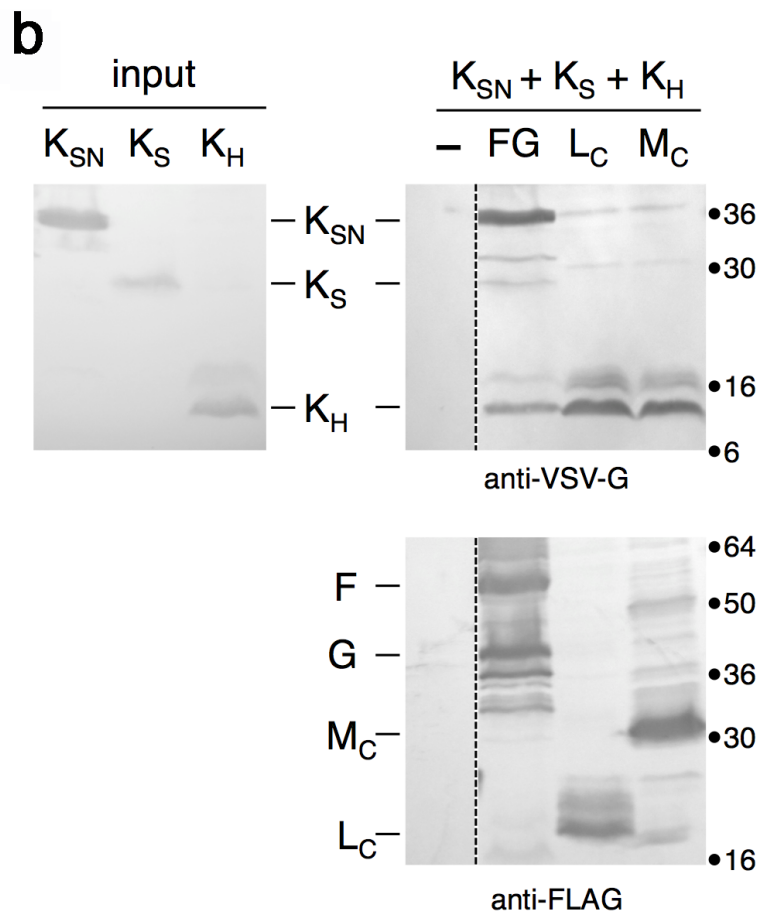
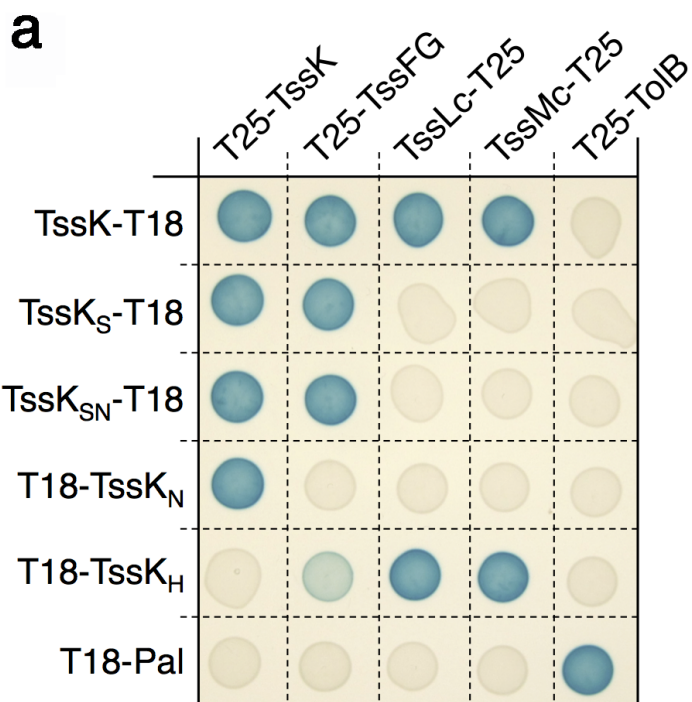


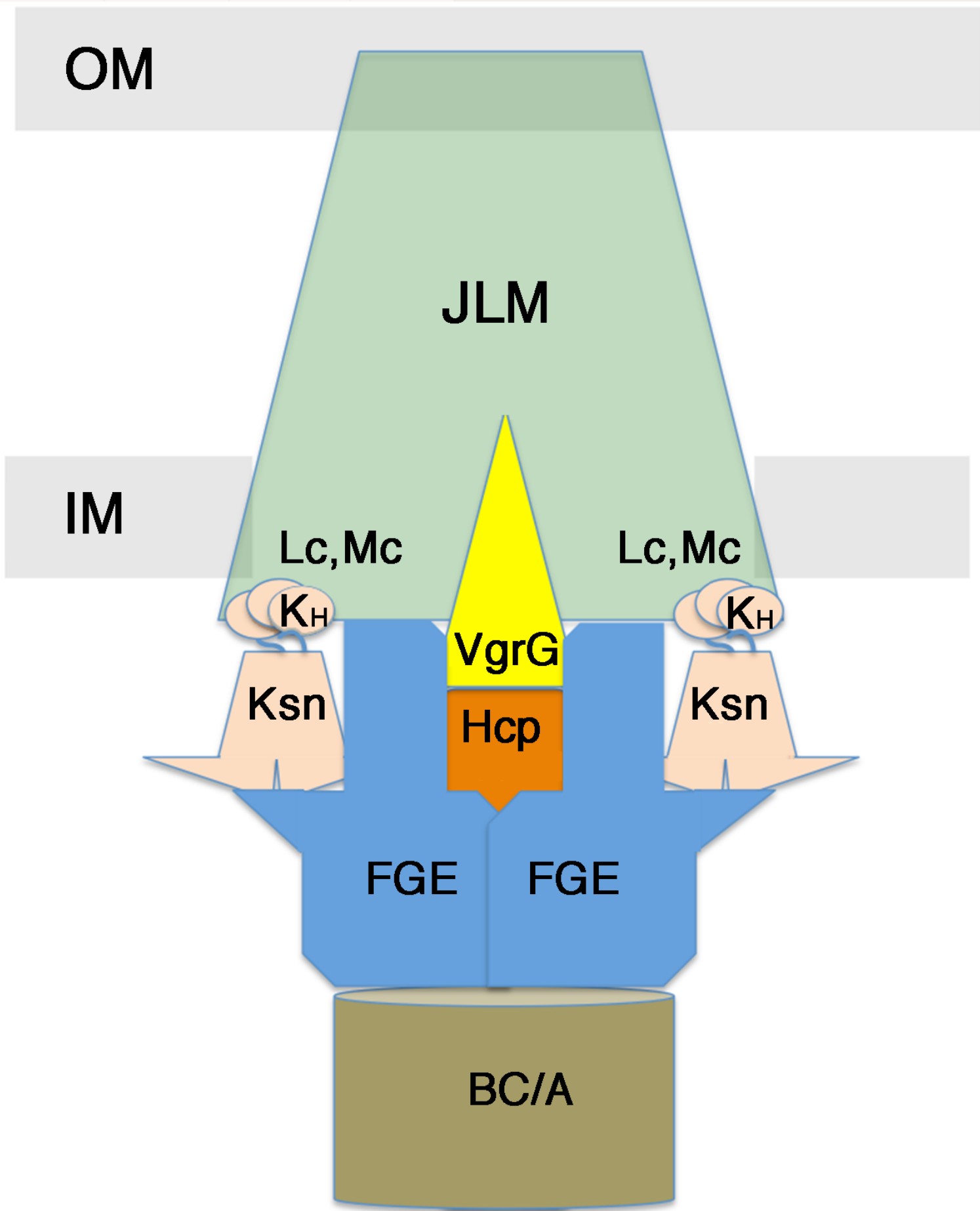


Nt

Ct

TssK- Nt
Phage1358-RBP-Nt
Phage p2-RBP-Nt





Type VI secretion TssK baseplate protein exhibits structural similarities with phage receptor binding protein and evolved to bind the membrane complex

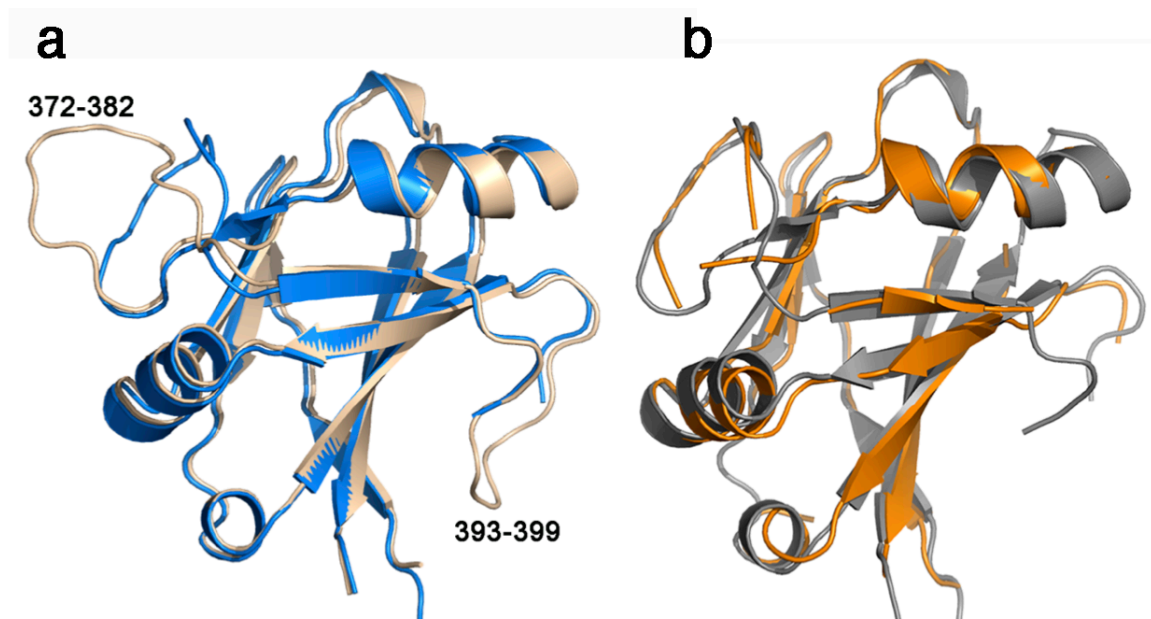
Van Son Nguyen, Laureen Logger, Silvia Spinelli, Pierre Legrand, Thi Thanh Huyen Pham, Thi Trang Nhung Trinh, Yassine Cherrak, Abdelrahim Zoued, Aline Desmyter, Eric Durand, Alain Roussel, Christine Kellenberger, Eric Cascales* and Christian Cambillau*

- corresponding authors: Eric Cascales (cascales@imm.cnrs.fr) and Christian Cambillau (cambillau@afmb.univ-mrs.fr).

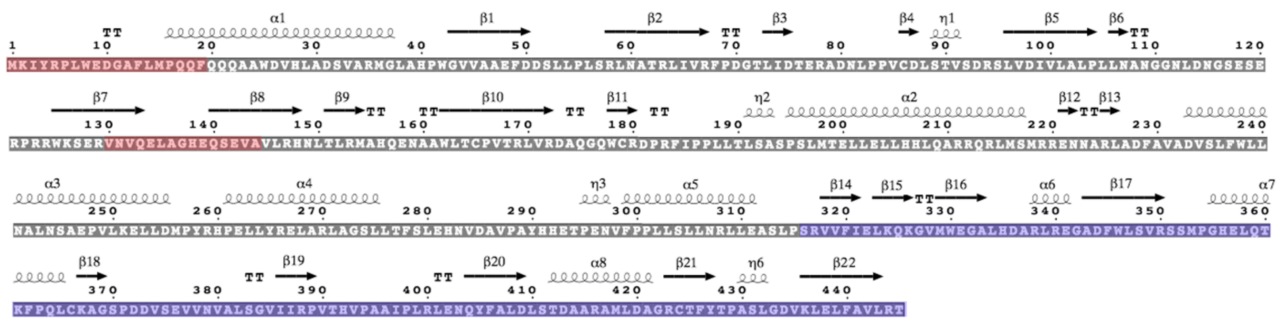
This PDF file includes:

Supplementary Figures 1-10

Supplementary Tables 1-3

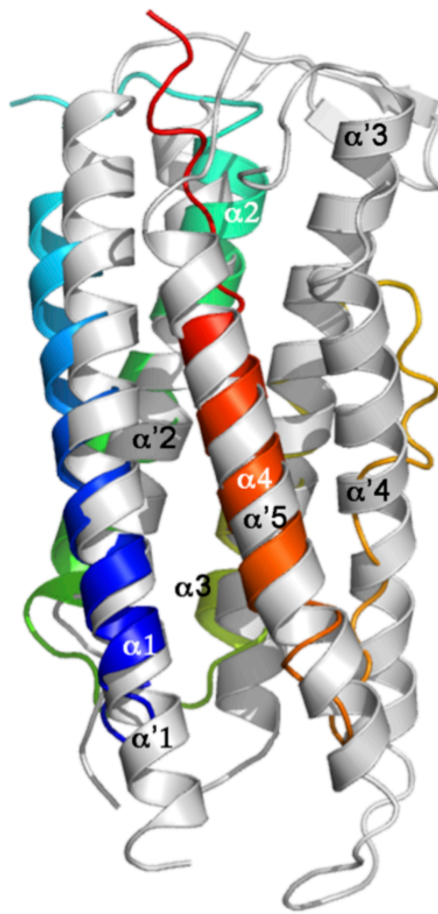


Supplementary Figure 2. Structural analysis of the TssK C-terminal domain. a, overlay between the TssK C-terminal head domain crystallized alone (beige) and in the refined full-length structure after insertion of the TssK C-terminal shoulder domain structure (blue). **b**, overlay between the TssK C-terminal head domain crystallized alone (grey) and in the full-length structure before the TssK C-terminal head structure insertion (orange).

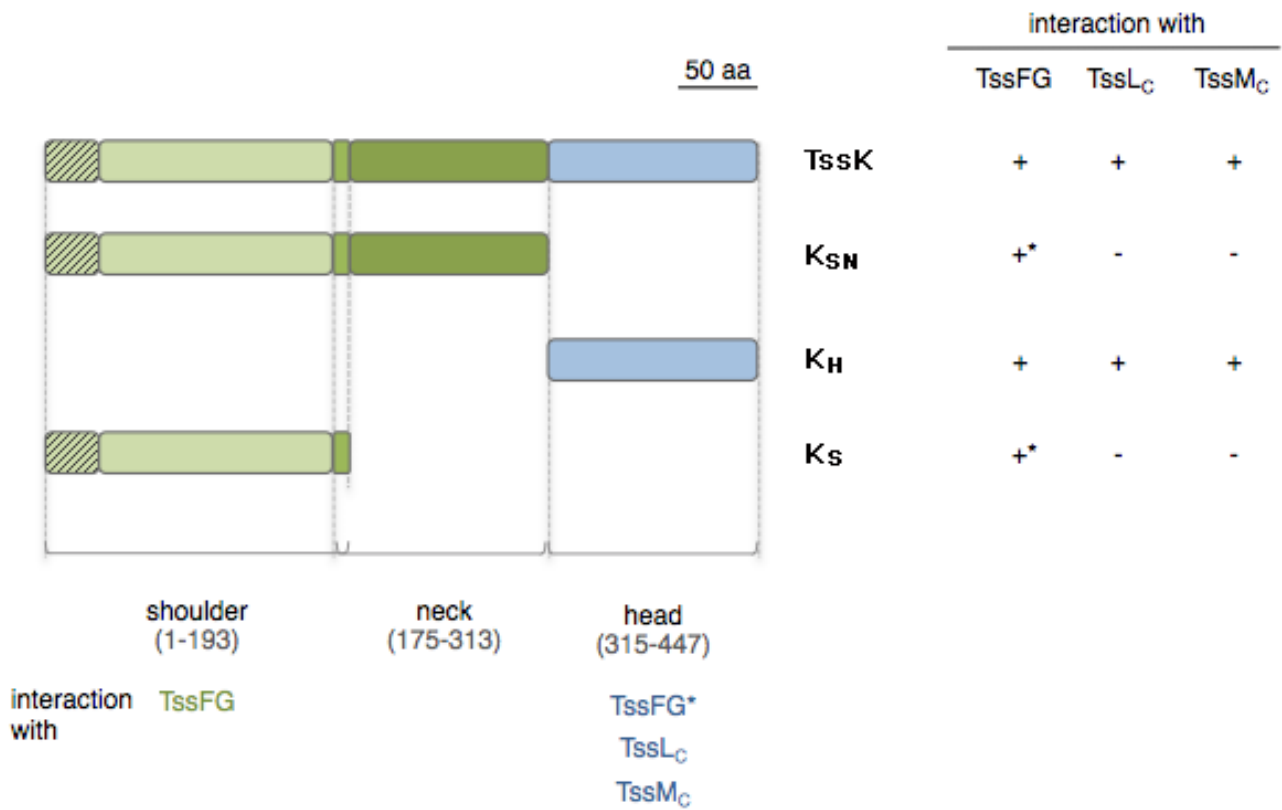


TssK+ nbK18 GVV GVI (subunit B only, high B-factors)
 TssK_{SN} GVI
 TssK_{SN}+ nbK18+nbK27 RPL GVV

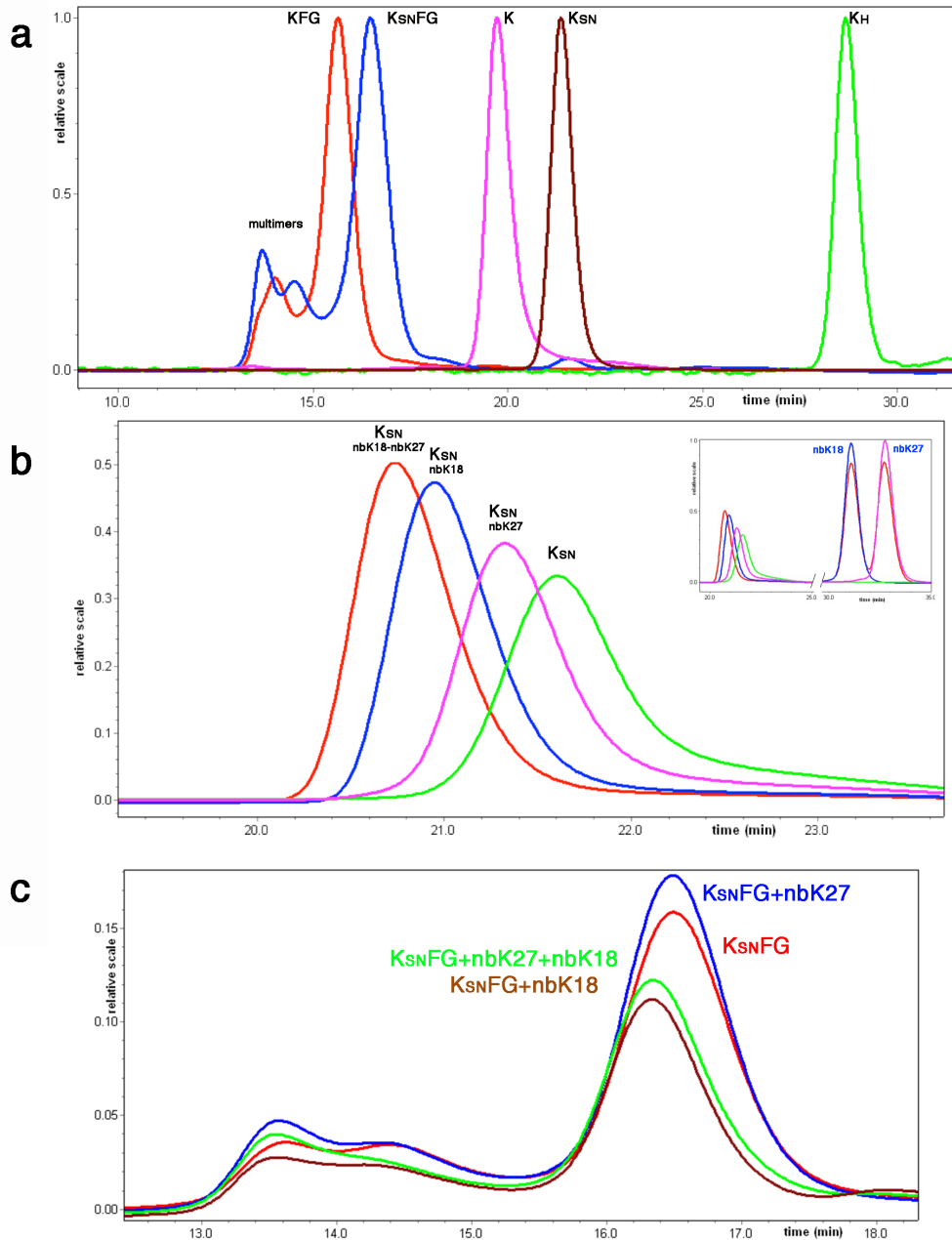
Supplementary Figure 3. Linear sequence representation of TssK with secondary structures. The domains or segments present in the different crystal structures are identified with different colors.



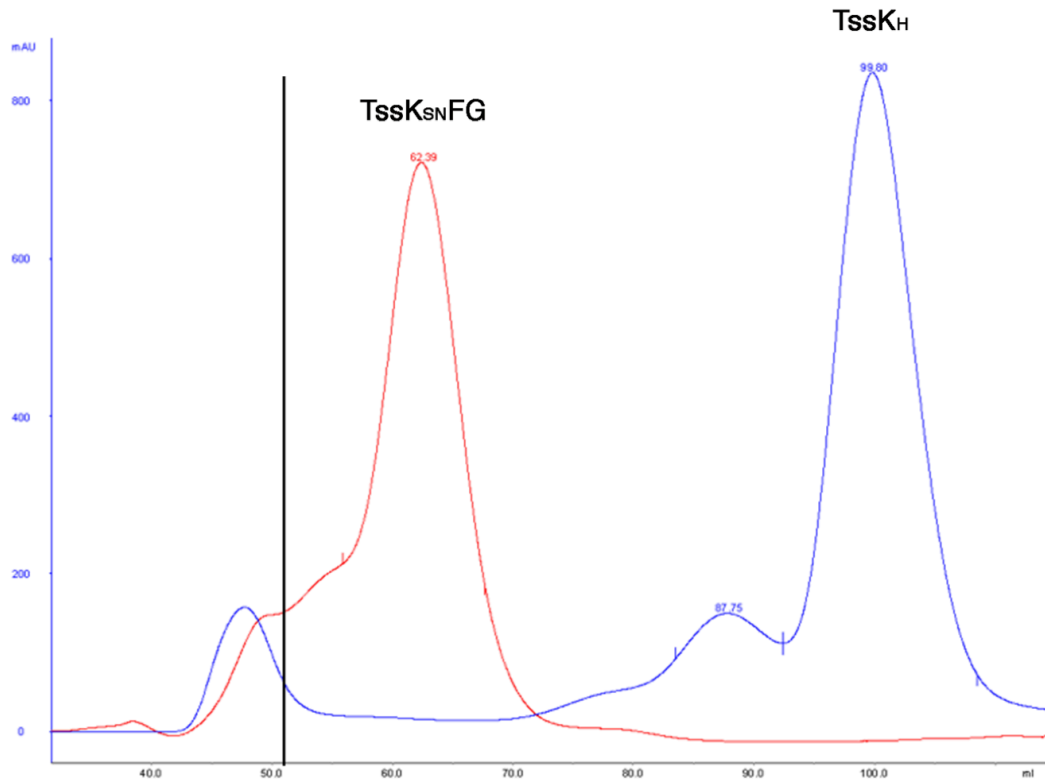
Supplementary Figure 4. Structural homologies of the TssK central domain (neck). Ribbon view of the overlay of t TssK_N helical bundle (rainbow colored) with the Human adenylosuccinate lyase (grey, PDB: 4FFX).



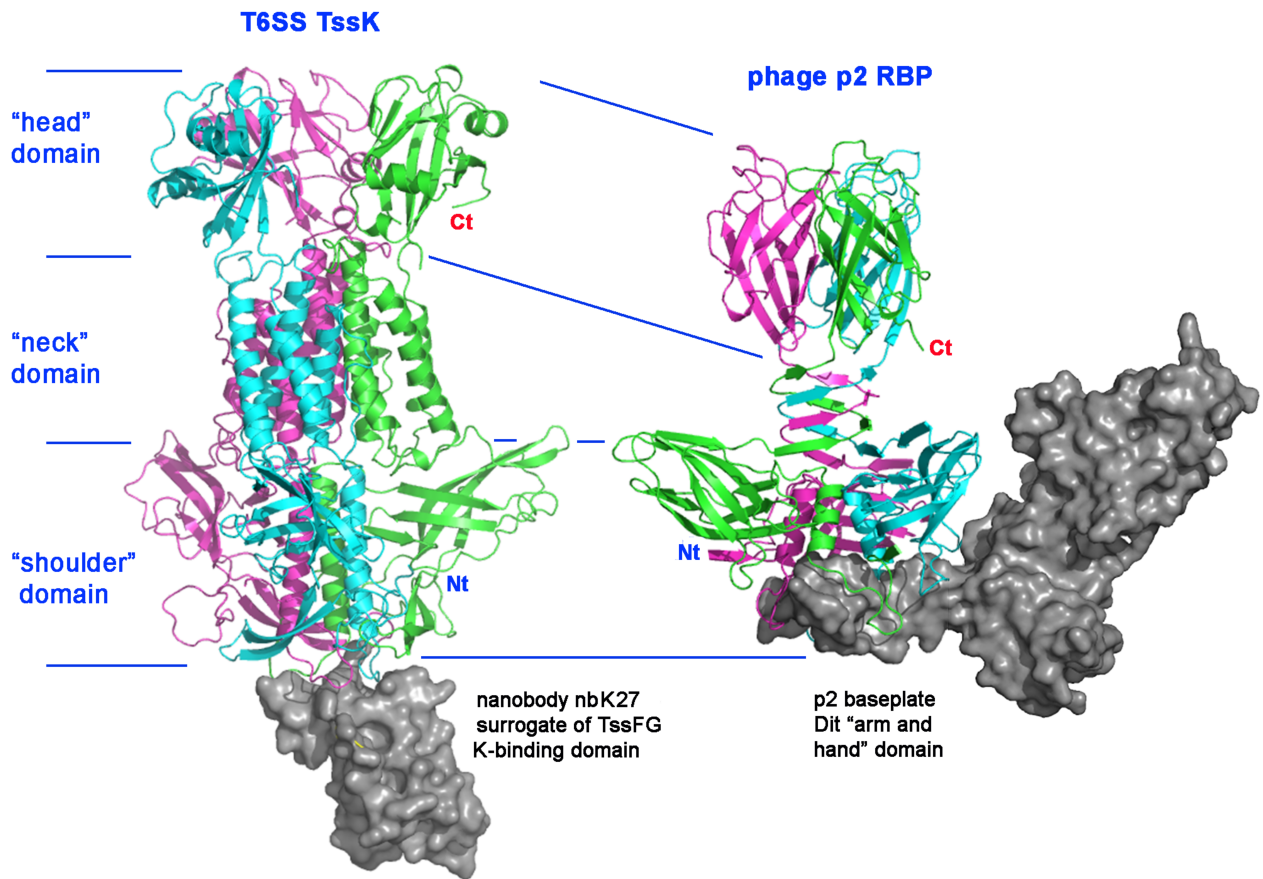
Supplementary Figure 5. Summary of the TssK domains interaction study. The different constructs used for the co-immunoprecipitation analyses are shown on left, with their boundaries (light green, N-terminal shoulder domain (K_S), amino-acids 1-193; dark green, central neck domain (K_N), amino-acids 175-313; blue, C-terminal head domain (K_H), amino-acids 315-447). The interactions identified by co-immunoprecipitations are indicated with '+' on the right (*, interaction observed by co-immunoprecipitation but not confirmed by co-purification and nanobody binding assays).



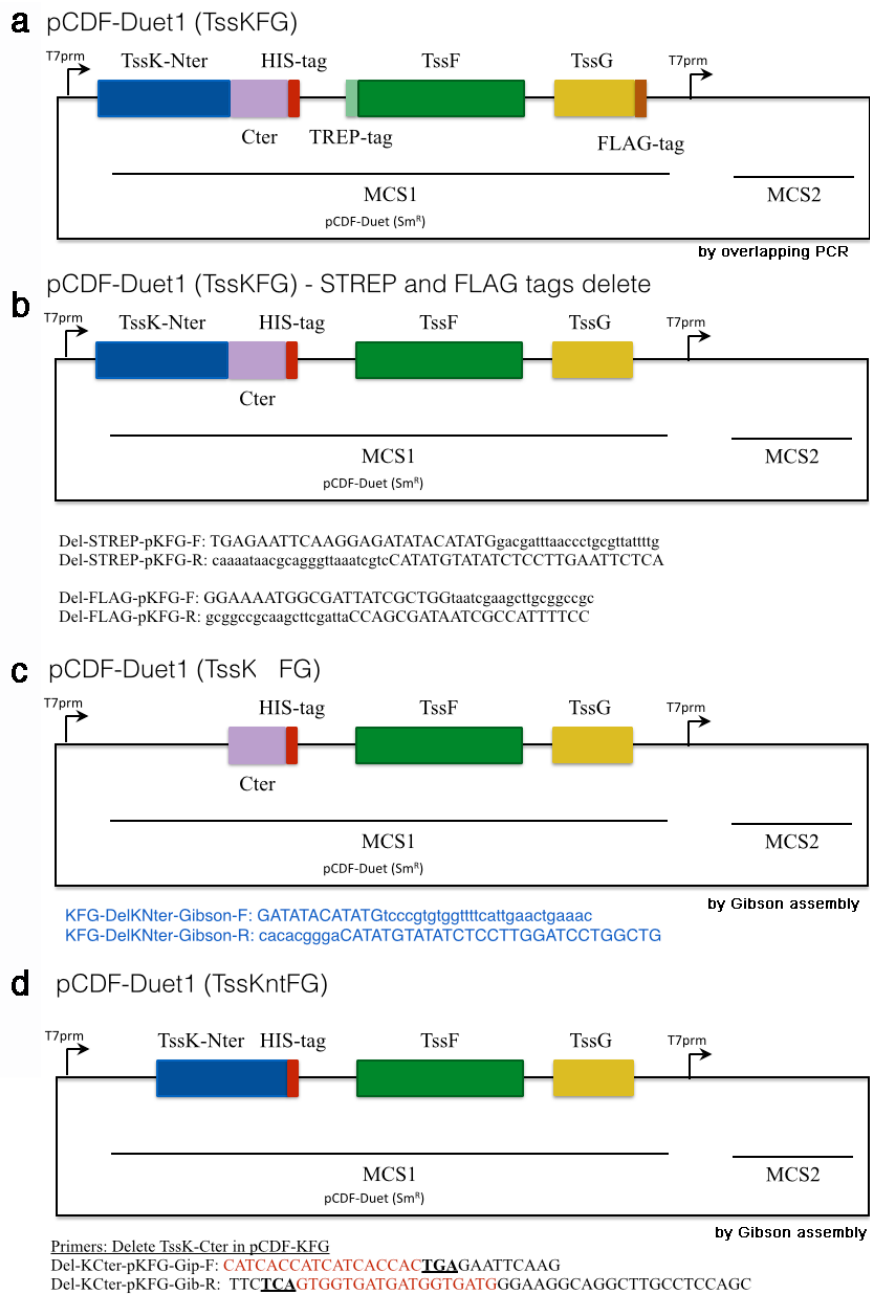
Supplementary Figure 6. **a**, HPLC gel Filtration chromatograms of TssKH, TssKSN, TssK, TssKSNFG and TssKFG. The peaks appearing before TssKFG are assigned to multimers. The peak amplitude has been scaled to 1.0. **b**, HPLC gel Filtration chromatograms of TssKSN in the presence of an excess of nbK18, nbK27 and nbK18, nbK27. **Inset**: the full chromatogram with the nanobodies. **c**, HPLC gel Filtration chromatograms of TssKSNFG alone or in the presence of an excess nbK27 of nbK18, and nbK18 + nbK27. **a,c**: the experiments were done in triplicate and a representative result is shown.



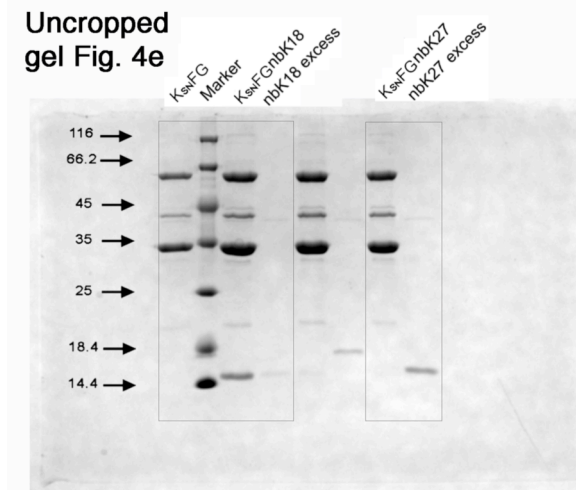
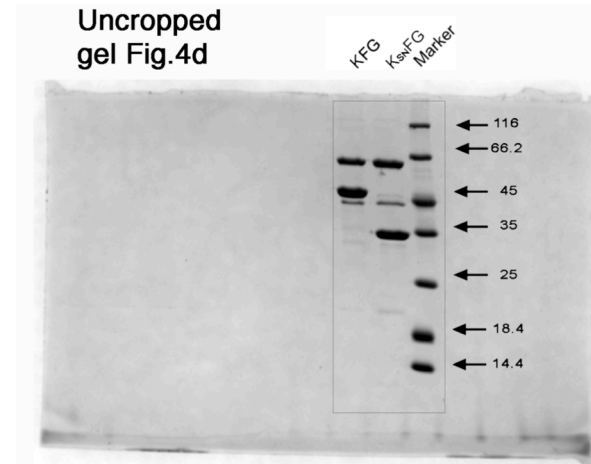
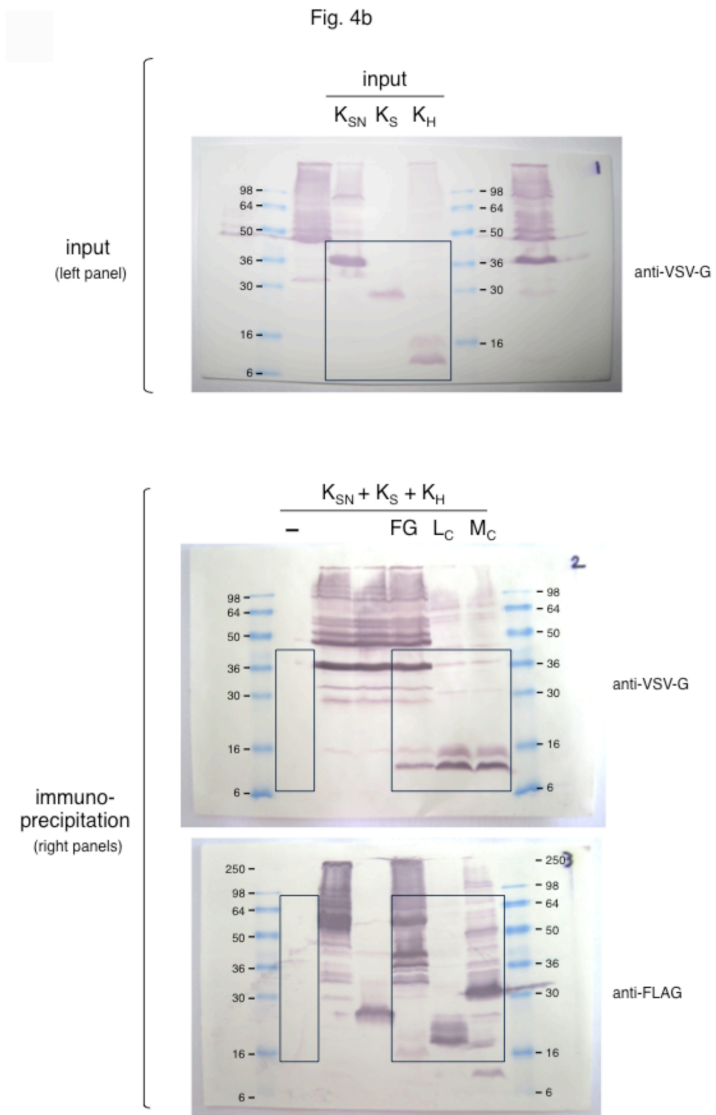
Supplementary Figure 7. Gel Filtration chromatograms of the product resulting from the *tssK_HFG* expression (blue) compared to the *tssK_{SNFG}* expression (orange). The main peak of the blue chromatogram corresponds to TssKH alone, indicating that a stable TssKHFG complex is not formed.



Supplementary Figure 8. Comparison of the TssK and phage p2 RBP structures evidencing the common topology of these trimers formed of shoulder, neck and head domains. The binding of TssK to nbK27 (that occupies the binding site of TssFG) is reminiscent of the binding of the Dit arm and hand extension of the phage p2 Dit molecule.



Supplementary Figure 9. Schematic representation of the *tssKFG* His, strep and flag (**a**), *tssKFG* His (**b**), *tssK_{SN}FG* (**c**) and *tssK_HFG* (**d**) constructs used in this study.



Supplementary Figure 10. Uncropped blots and gels.

Supplementary Table 1. Data collection and refinement statistics of nbK18, nbK18-TssK and TssK_{SN}-nbK18-nbK27 complexes, and TssK_H domain. (numbers in brackets refer to the highest resolution bin)

DATA COLLECTION	nbK18	TssK-nbK18 CsI/NaI	TssK-nbK18 native	TssK _{SN} -nbK18- nbK27	TssK _H
PDB	5M2W		5M30	5MWN	5M2Y
Source	ESRF ID23-2	Soleil PX 1	Soleil PX 1	ESRF ID30A-3	ESRF ID23-1
Wavelength (Å)	0.9786	1.7712	0.9786	0.9677	0.9789
Space group	P4 ₃	P2 ₁ 2 ₁ 2 ₁	P2 ₁ 2 ₁ 2 ₁	P2 ₁ 2 ₁ 2 ₁	P3 ₂
Cell (Å)	a=b=53.4 Å, c = 88.0 Å	a=93.4, b=153.7 c=154.2	a=93.2, b=153.7, c=154.8	a=90.9, b=143.3, c=150.3	a=b=63.8, c=63.1
Angles (°)	$\alpha=\beta=\gamma=90$	$\alpha=\beta=\gamma=90$	$\alpha=\beta=\gamma=90$	$\alpha=\beta=\gamma=90$	$\alpha=\beta=90$;
Nr. of monomers	2	3/3	3/3	3/3/1	2
Resolution limits (Å)	20-1.50 (1.59-1.5)	50-3.49 (3.6-3.49)	50.0-2.6 (2.66-2.6)	50.0-2.20 (2.33-2.20)	41.6-1.61 (1.71-1.61)
Rmerge (Rpim ^a)	0.088 (0.785)	0.016 (1.8)	0.018 (1.40) ^a	0.077 (0.84)	0.06 (0.65)
CC1/2	0.994 (0.61)	0.999 (0.32)	1.0 (0.30)	0.993 (0.5)	0.99 (0.90)
Unique reflections	38858 (6348)	54138	69265 (4986)	100494 (16357)	36972 (5934)
Mean(I)/sd(I)	7.8 (1.6)	14.6 (1.0)	19.6 (0.5)	6.5 (1.0)	22.79 (3.36)
Completeness (%)	98.7 (98.2)	100 (99.5)	99.8 (99.2)	95.5 (92.4)	99.9 (99.5)
Multiplicity	3.5 (3.3)	18 (8)	11.0 (10.7)	4.8 (4.4)	10.6 (10.5)
SigAno (4.18 Å)		7.9 (0.94)			
CCano (4.18 Å)		0.98 (0.14)			
REFINEMENT					
Resolution (Å)	12.1-1.5 (1.54-1.5)		48.9-2.6 (2.67-2.6)	45.0-2.20 (2.26-2.20)	12.7-1.61 (1.65 1.61)
Number of reflections	38782 (2908)		59771 (4503)	98369 (6904)	36903 (2686)
Number of protein / water / ions atoms	1712/296/15		10297/120	10822/694	1966/223
Test set reflections	1940 (146)		2988	5032	1845
R _{work} /R _{free}	0.195/0.212 (0.3/0.28)		0.198/0.218 (0.249/0.295)	0.199/0.220 (0.232/0.249)	0.198/0.199 (0.216/0.246)
r.m.s.d.bonds (Å)/angles (°)	0.011 / 1.13		0.009 / 1.09	0.008 / 1.07	0.012 / 1.12
B-Wilson / B-mean Å	22.7 / 28.6		108.5/107.1	57.1/66.4	25.7/32.2
Ramachandran: preferred / allowed / outliers (%)	96.3 / 3.7 / 0		97.1/2.6/0.3	79.9/2.1/0	98.0/2.0/0

Supplementary Table 2. Interaction contacts between TssK and the nbK18 nanobody (obtained with the PISA server (Krissinel & Henrick, 2007)). ASA: accessible surface area (\AA^2). BSA: buried surface area (\AA^2). **a)** surface of nbK18; blue: CDR1; green: CDR2; pink: CDR3. **b)** surface of TssK. (The bars indicate the percentage of the ASA covered; 1 bar = 10%).

a)

	H-bonds	ASA	BSA
VAL 32		56.25	42.21
VAL 33		37.25	32.81
ALA 35		8.52	8.37
TYR 37	H	41.54	25.97
total			125
LEU 47		79.47	60.17
SER 50		18.33	10.61
THR 52	H	49.89	18.84
GLY 54		75.43	13.20
THR 56	H	86.79	9.83
ALA 60		21.75	13.55
total			132
LYS 96	H	33.05	22.99
PHE 98		73.41	72.20
ARG 100	H	133.07	69.68
TYR 103		188.69	110.41
VAL 104		79.31	32.53
GLY 105	H	38.52	38.52
TYR 106		89.32	33.59
ASP 107	H	79.14	65.47
total			452
Grand total			709

b)

	H-bonds	ASA	BSA
PRO 69		47.50	37.02
ASP 70		44.65	21.34
LEU 105		78.77	78.45
LEU 106	H	70.66	33.60
ASN 107	H	42.33	36.39
ALA 108	H	106.15	35.88
ASN 109	H	149.19	58.67
GLY 110		39.76	11.02
GLU 118		170.72	61.86
SER 119		48.16	17.95
GLU 120	H	165.08	139.61
ARG 121		54.64	43.11
GLU 158	H	160.85	84.97
ALA 160	H	97.20	48.41
ALA 161		35.99	24.80
TRP 162	H	48.61	8.76
LEU 163		22.45	21.13

Supplementary Table 3. Strains, plasmids and oligonucleotides used in this study.

Strains

Strains	Description and genotype	Source
<i>E. coli</i> K-12		
DH5 α	F-, $\Delta(\text{argF-lac})$ U169, <i>phoA</i> , <i>supE44</i> , $\Delta(\text{lacZ})$ M15, <i>relA</i> , <i>endA</i> , <i>thi</i> , <i>hsdR</i>	New England Biolabs
W3110	F-, lambda- IN(<i>rrnD-rrnE</i>)1 <i>rph-1</i>	Laboratory collection
BTH101	F-, <i>cya-99</i> , <i>araD139</i> , <i>galE15</i> , <i>galK16</i> , <i>rpsL1</i> (<i>Str r</i>), <i>hsdR2</i> , <i>mcrA1</i> , <i>mcrB1</i> .	Karimova <i>et al.</i> , 2005
T7 Iq pLys	MiniF, <i>lysY</i> , <i>lacI^H</i> (Cam ^R), <i>fhuA2</i> , <i>lacZ::T7 gene1</i> , <i>ompT</i> , <i>gal</i> , <i>sulA11</i> , <i>R(mcr-73::miniTn10--Tet^S)2</i> , <i>dcm</i> , <i>R(zgb-210::Tn10--Tet^S)</i> <i>endA1</i> $\Delta(\text{mcrC-mrr})$	New England Biolabs
Enteroaggregative <i>E. coli</i>		
17-2	WT enteroaggregative <i>Escherichia coli</i>	Arlette Darfeuille-Michaud

Plasmids

Vectors	Description	Source
Protein production vectors		
pRSF-1	cloning vector, <i>PT7</i> , Kan ^R	Novagen
pRSF-TssK _{6His}	<i>sci-1 tssK</i> cloned into pRSF-1, C-terminal 6×His sequence	This study
pETG20A	Gateway® destination vector, 6×His-TRX followed by a TEV cleavage site	Arie Geerlof
pETG-TssK _{Ct}	<i>sci-1 tssK</i> residues 316-445 cloned into pETG20A	This study
Expression vectors		
pASK-IBA37	cloning vector, <i>Ptet</i> , Amp ^R	IBA Technology
pASK-IBA37-TssA _{FLAG}	<i>sci-1 tssA</i> cloned into pASK-IBA37, C-terminal FLAG epitope	Zoued <i>et al.</i> , 2016
pASK-IBA37-TssF _{FLAG}	<i>sci-1 tssF</i> cloned into pASK-IBA37, C-terminal FLAG epitope	Brunet <i>et al.</i> , 2015
pASK-IBA37-TssG _{FLAG}	<i>sci-1 tssG</i> cloned into pASK-IBA37, C-terminal FLAG epitope	Brunet <i>et al.</i> , 2015
pASK-IBA37- _{FLAG} TssLc	<i>sci-1 tssL</i> residues 1-184 cloned into pASK-IBA37, N-terminal FLAG epitope	Aschtgen <i>et al.</i> , 2012
pASK-IBA37-TssM _C -NTP _{FLAG}	<i>sci-1 tssM</i> residues 62-273 cloned into pASK-IBA37, C-terminal FLAG epitope	Logger <i>et al.</i> , 2016
pBAD33	cloning vector, pACYC184 origin, <i>Para</i> , <i>araC</i> , Cm ^R	Guzman <i>et al.</i> , 1995
pBAD33-TssK _{VSV-G}	<i>sci-1 tssK</i> cloned into pBAD33, C-terminal VSV-G epitope	Brunet <i>et al.</i> , 2015
pBAD33-TssK-SN _{VSV-G}	<i>sci-1 tssK</i> residues 1-315 cloned into pBAD33, C-terminal VSV-G epitope	This study
pBAD33-TssK-H _{VSV-G}	<i>sci-1 tssK</i> residues 315-445 cloned into pBAD33, C-terminal VSV-G epitope	This study
pBAD33-TssK-S _{VSV-G}	<i>sci-1 tssK</i> residues 1-193 cloned into pBAD33, C-terminal VSV-G epitope	This study
pBAD33-TssK-N _{VSV-G}	<i>sci-1 tssK</i> residues 175-315 cloned into pBAD33, C-terminal VSV-G epitope	This study
pUC-Hcp _{FLAG}	<i>sci-1 hcp</i> cloned into pUC12, <i>Plac</i> , C-terminal FLAG epitope	Aschtgen <i>et al.</i> , 2008

Bacterial Two-Hybrid vectors		
pT18-FLAG	Bacterial Two Hybrid vector, ColE1 origin, <i>Plac</i> , T18 fragment of <i>Bordetella pertussis</i> CyaA, Amp ^R	Battesti & Bouveret, 2008
pTssK-T18	<i>tssK</i> cloned upstream T18 in pT18-FLAG	Zoued <i>et al.</i> , 2013
pTssK _S -T18	<i>tssK</i> residues 1-193 cloned upstream T18 in pT18-FLAG	This study
pT18-TssK _N	<i>tssK</i> residues 175-315 cloned downstream T18 into pT18-FLAG	This study
pTssK _{SN} -T18	<i>tssK</i> residues 1-315 cloned upstream T18 into pT18-FLAG	This study
pT18-TssK _H	<i>tssK</i> residues 315-445 cloned downstream T18 into pT18-FLAG	This study
pT18-Pal	<i>pal</i> cloned downstream the T18 coding sequence in pT18-FLAG	Battesti & Bouveret, 2008
pT25-FLAG	Bacterial Two Hybrid vector, p15A origin, <i>Plac</i> , T25 fragment of <i>Bordetella pertussis</i> CyaA, Kan ^R	Battesti & Bouveret, 2008
pT25-TssFG	<i>tssFG</i> cloned downstream the T25 coding sequence in pT25-FLAG	Brunet <i>et al.</i> , 2015
pT25-TssK	<i>tssK</i> cloned downstream the T25 coding sequence in pT25-FLAG	Zoued <i>et al.</i> , 2013
pTssL _C -T25	<i>tssL</i> residues 1-184 cloned downstream the T25 coding sequence in pT25-FLAG	Durand <i>et al.</i> , 2012
pTssM _C -T25	<i>tssM</i> residues 62-360 cloned upstream the T25 coding sequence in pT25-FLAG	Zoued <i>et al.</i> , 2013
pT25-TolB	<i>tolB</i> cloned upstream the T25 coding sequence in pT25-FLAG	Battesti & Bouveret, 2008

Oligonucleotides

Name	Destination	Sequence (5' → 3')
For plasmid construction ^{b,c,d}		
5- pBAD33-TssK-SN _{VSV-G}	insertion of <i>tssK</i> ₁₋₃₁₅ fragment into pBAD33	<u>CTCTCTACTGTTTCTCCATAACCCGTTTTTTTTGGGCT</u> <u>AGCAGGAGGTATTACACCATGAAGATTTATCGCCCA</u> TTATGGGAAGACG
3- pBAD33-TssK-SN _{VSV-G}	insertion of <i>tssK</i> ₁₋₃₁₅ fragment into pBAD33	GGTCGACTCTAGAGGATCCCCGGGTACCTTATTT TCCTAATCTATTCATTTCAATATCTGTATAGGAAGG CAGGCTTGCCTCCAGC
5- pBAD33-TssK-H _{VSV-G}	insertion of <i>tssK</i> ₃₁₅₋₄₄₅ fragment into pBAD33	<u>CTCTCTACTGTTTCTCCATAACCCGTTTTTTTTGGGCT</u> <u>AGCAGGAGGTATTACACCATGCGTGTGG</u> TTTTCAATTGAACTGAAACAAAAGGC
3- pBAD33-TssK-H _{VSV-G}	insertion of <i>tssK</i> ₃₁₅₋₄₄₅ fragment into pBAD33	GGTCGACTCTAGAGGATCCCCGGGTACCTTATTT TCCTAATCTATTCATTTCAATATCTGTATATGT CCGCAGCACCGCAAAAAGTTC
3-pBAD33-TssK-S _{VSV-G}	insertion of <i>tssK</i> ₁₋₁₉₃ fragment into pBAD33	<u>GGTCGACTCTAGAGGATCCCCGGGTACCTTA</u> <u>TTTTCCTAATCTATTCATTTCAATATCTGTATA</u> GGCAGACAGCGTCAGCAGAGGG
5-pBAD33-TssK-N _{VSV-G}	insertion of <i>tssK</i> ₁₇₅₋₃₁₅ fragment into pBAD33	<u>CTCTCTACTGTTTCTCCATAACCCGTTTTTTTTGGGCT</u> <u>AGCAGGAGGTATTACACCATGGGACAGTGG</u> TGCAGGGACCCGCG
5-pTssK _S -T18	insertion of <i>tssK</i> ₁₋₁₉₃ fragment into pT18-Flag	<u>CGGATAACAATTTACACAGGAAACAGCTATGACC</u> <u>ATGAAGATTTATCGCCATTATGGGAAGACG</u>
3-pTssK _S -T18	insertion of <i>tssK</i> ₁₋₁₉₃ fragment into pT18-Flag	CCTCGCTGGCGGCTAAGCTTGGCGTAAT GGCAGACAGCGTCAGCAGAGGG
5-pT18-TssK _N	insertion of <i>tssK</i> ₁₇₅₋₃₁₅ fragment into pT18-Flag	<u>GCCACTGCAGGGATTATAAAGATGACGATGA</u> <u>CAAGGGACAGTGGTGCAGGGACCCGC</u>
3-pT18-TssK _N	insertion of <i>tssK</i> ₁₇₅₋₃₁₅ fragment into pT18-Flag	AGGTCGACGGTATCGATAAGCTTGATATCGAATTC

		<u>TAGTTAGGAAGGCAGGCTTGCCTCCAGC</u>
5-pTssK _{SN} -T18	insertion of <i>tssK</i> ₁₋₃₁₅ fragment into pT18-Flag	<u>CGGATAACAATTTACACAGGAAACAGCTATGACC</u> <u>ATGAAGATTTATCGCCCATTATGGGAAGACG</u>
3-TssK _{SN} -T18	insertion of <i>tssK</i> ₁₋₃₁₅ fragment into pT18-Flag	<u>CCTCGCTGGCGGCTAAGCTTGGCGTAATGGAAG</u> <u>GCAGGCTTGCCTCCAGC</u>
5-pT18-TssK _H	insertion of <i>tssK</i> ₃₁₅₋₄₄₅ fragment into pT18-Flag	<u>CGCCACTGCAGGGATTATAAAGATGACGATGACA</u> <u>AGCGTGTGGTTTTTCATTGAACTGAAACAAAAGGG</u>
3-pT18-TssK _H	insertion of <i>tssK</i> ₃₁₅₋₄₄₅ fragment into pT18-Flag	<u>CGAGGTCGACGGTATCGATAAGCTTGATATCGAA</u> <u>TTCTAGTTATGTCCGCAGCACCGCAAAAAGTTC</u>
T6_K316-445_p17_F	insertion of <i>tssK</i> ₃₁₆₋₄₄₅ fragment into pETG20A	<u>GGCTTAGAAAACCTGTACTTCCAGGGTTCCCGT</u> <u>GTGGTTTTTCATTGAACTGAAAC</u>
T6_K316-445_p17_R	insertion of <i>tssK</i> ₃₁₆₋₄₄₅ fragment into pETG20A	<u>ACCACTTTGTACAAGAAAGCTGGGTTTATTATGTCC</u> <u>GCAGCACCGCAAAAAGTTCC</u>

^a Sequence annealing on the target plasmid underlined.

^b VSV-G epitope coding sequence *italicized*.